

Progress of Theoretical Physics, Vol. 123, No. 1, January 2010

Theoretical Foundation of the Nuclear Force in QCD and Its Applications to Central and Tensor Forces in Quenched Lattice QCD Simulations

Sinya AOKI,¹ Tetsuo HATSUDA² and Noriyoshi ISHII²

¹*Graduate School of Pure and Applied Sciences, University of Tsukuba,
Tsukuba 305-8571, Japan*

²*Department of Physics, University of Tokyo,
Tokyo 113-0033, Japan*

(Received October 5, 2009)

We present full accounts of a method to extract nucleon-nucleon (NN) potentials from the Bethe-Salpter amplitude in lattice QCD. The method is applied to two nucleons on the lattice with quenched QCD simulations. By disentangling the mixing between the S-state and the D-state, we obtain central and tensor potentials in the leading order of the velocity expansion of the non-local NN potential. The spatial structure and the quark mass dependence of the potentials are analyzed in detail.

Subject Index: 164, 232, 234

§1. Introduction

The origin of the nuclear force is one of the major unsolved problems in particle and nuclear physics even after the establishment of the quantum chromodynamics (QCD). Although the nuclear force is still not well-understood theoretically, a large number of proton-proton and neutron-proton scattering data as well as deuteron properties have been accumulated and summarized e.g. in the Nijmegen database.¹⁾ To describe the elastic nucleon-nucleon (NN) scattering at low-energies below the pion production threshold together with the deuteron properties, the notion of the NN potential (either in the coordinate space or in the momentum space) turns out to be very useful:²⁾ it can be determined phenomenologically to reproduce the scattering phase shifts and bound state properties either through the Schrödinger equation for the NN wave function or through the Lippmann-Schwinger equation for the NN T -matrix. Once the potential is determined, it can be used to study systems with more than 2 nucleons by using various many-body techniques.

Phenomenological NN potentials which can fit the NN data precisely (e.g. more than 2000 data points with $\chi^2/\text{dof} \simeq 1$) at $T_{\text{lab}} < 300$ MeV are called the high-precision NN potentials: They include the potentials such as CD-Bonn,³⁾ Argonne v_{18} ,⁴⁾ and Nijm I, Nijm II and Reid93.⁵⁾ Also systematic low energy construction of the nuclear force on the basis of the chiral perturbation theory is being developed.^{6),7)}

The phenomenological NN potentials in the coordinate space are known to reflect some characteristic features of the NN interaction at different length scales:²⁾

- (i) The long range part of the nuclear force (the relative distance $r > 2$ fm) is dominated by the one-pion exchange introduced by Yukawa.⁸⁾ Because of the

pion's Nambu-Goldstone character, it couples to the spin-isospin density of the nucleon and hence leads to a strong spin-isospin dependent force, namely the tensor force.

- (ii) The medium range part ($1 \text{ fm} < r < 2 \text{ fm}$) receives significant contributions from the exchange of two-pions ($\pi\pi$) and heavy mesons (ρ , ω , and σ). In particular, the spin-isospin independent attraction of about $50 - 100 \text{ MeV}$ in this region plays an essential role for the binding of atomic nuclei.
- (iii) The short range part ($r < 1 \text{ fm}$) is best described by a strong repulsive core as originally introduced by Jastrow.⁹⁾ Such a short range repulsion is important for the stability of atomic nuclei against collapse, for determining the maximum mass of neutron stars, and for igniting the Type II supernova explosions.¹⁰⁾
- (iv) There is also a strong attractive spin-orbit force in the isospin 1 channel at medium and short distances. This leads to the ${}^3\text{P}_2$ neutron pairing in neutron matter and hence the neutron superfluidity inside neutron stars.¹⁰⁾

A repulsive core surrounded by an attractive well is in fact a common feature of the “effective” potential between composite particles. The Lenard-Jones potential between neutral atoms or molecules is a well-known example in atomic physics. The potential between ${}^4\text{He}$ nuclei is a typical example in nuclear physics. The origin of the repulsive cores in these examples is known to be the Pauli exclusion among electrons or among nucleons. The same idea, however, is not directly applicable to the NN potential, because the quark has not only spin and flavor but also color which allows six quarks to occupy the same state without violating the Pauli principle. To account for the repulsive core of the NN force, therefore, various ideas have been proposed as summarized in Ref. 11): exchange of the neutral ω meson,¹²⁾ exchange of non-linear pion field,¹³⁾ and a combination of the Pauli principle with the one-gluon-exchange between quarks.¹⁴⁾ Despite all these efforts, convincing account of the nuclear force has not yet been obtained.

In this situation, it is highly desirable to study the NN interactions from the first principle lattice QCD simulations. A theoretical framework suitable for such purpose was first proposed by Lüscher:¹⁵⁾ For two hadrons in a finite box with the size $L \times L \times L$ in periodic boundary conditions, an exact relation between the energy spectra in the box and the elastic scattering phase shift at these energies was derived: If the range of the hadron interaction R is sufficiently smaller than the size of the box $R < L/2$, the behavior of the two-particle Bethe-Salpeter (BS) wave function $\psi(\mathbf{r})$ in the interval $R < |\mathbf{r}| < L/2$ under the periodic boundary conditions has sufficient information to relate the phase shift and the two-particle spectrum.

Lüscher's method bypasses the difficulty to treat the real-time scattering process on the Euclidean lattice.^{*)} Furthermore, it utilizes the finiteness of the lattice box effectively to extract the information of the on-shell scattering matrix and the phase shift. This approach has been applied to extract the NN scattering lengths in the

*) There are several studies of the NN interactions on the lattice, which do not rely on Lüscher's method. One uses the Born-Oppenheimer picture, i.e., if one of the three quarks inside the baryon is infinitely heavy, one may define the potential between baryons a la Born-Oppenheimer.¹⁶⁾ This is, however, not applicable to the nucleons with light quarks. The other employs the strong coupling limit, which has been proposed quite recently.¹⁷⁾

quenched QCD simulations¹⁸⁾ and in the (2+1)-flavor QCD simulations with the mixed action.¹⁹⁾

Recently, the present authors proposed a closely related but an alternative approach to the NN interactions from lattice QCD.^{20),21)} The starting point is the same BS wave function $\psi(\mathbf{r})$ as discussed in Ref. 15). Instead of looking at the wave function outside the range of the interaction, we consider the internal region $|\mathbf{r}| < R$ and define the energy-independent non-local potential $U(\mathbf{r}, \mathbf{r}')$ from $\psi(\mathbf{r})$ so that it obeys the Schrödinger type equation in a finite box. Since $U(\mathbf{r}, \mathbf{r}')$ for strong interaction is localized in its spatial coordinates due to confinement of quarks and gluons, the potential receives finite volume effect only weakly in a large box. Therefore, once U is determined and is appropriately extrapolated to $L \rightarrow \infty$, one may simply use the Schrödinger equation in the infinite space to calculate the scattering phase shifts and bound state spectra to compare with experimental data. Further advantage of utilizing the potential is that it would be a smooth function of the quark masses so that it is relatively easy to handle on the lattice. This is in sharp contrast to the scattering length which shows a singular behavior around the quark mass corresponding to the formation of the NN bound state.^{*)}

Since we consider the non-asymptotic region ($|\mathbf{r}| < R$) of the wave function, the resultant potential U and the T -matrix are off-shell. Therefore, they depend on the nucleon interpolating operator adopted to define the BS wave function. This is in a sense an advantage, since one can establish a one-to-one correspondence between the nucleon interpolating operator and the NN potential in QCD, which is not attainable in phenomenological NN potentials. It also implies that the NN potential on the lattice and the phenomenological NN potentials are equivalent only in the sense that they give the same observables, so that the comparison of their spatial structures should be made only qualitatively.

The purpose of this paper is twofold: First, we will present a theoretical foundation of our method to extract the NN potentials from lattice QCD. Then, we will give a full account of the application of the method to the quenched lattice QCD simulations. Once our method in lattice QCD is proved to work in the NN system, it will have various applications not only to nuclear many-body problems but also to hyperon-nucleon, hyperon-hyperon and three-nucleon interactions which have much less experimental information than the NN systems. A first attempt to the hyperon-nucleon potential has been already reported in Ref. 24), and more on hyperons will appear in the future publications.

This paper is organized as follows. In §2, we illustrate the derivation of the two-body and many-body potentials from the wave function in quantum mechanics. In §3, the idea in the previous section is generalized to the interaction of composite particles in field theory. In §4, we classify the general structure of the NN potential in the velocity expansion and show the procedure to determine each term. In §5, the method to determine the NN potential from the lattice QCD data is discussed in

^{*)} Similar situation is well-studied in connection with the BEC-BCS crossover in cold fermionic atoms,²²⁾ where the external magnetic field plays a role of the quark mass in QCD. For seminal suggestion on the rapid quark-mass dependence of the NN scattering length, see Ref. 23).

detail for the effective central potential at low energy. We also discuss the method to extract the tensor potential in our approach. In §6, NN potentials obtained from the quenched lattice QCD simulations are presented. Section 7 is devoted to summary and concluding remarks. In Appendix A, a field-theoretical derivation of the asymptotic BS wave function at large distance is presented. In Appendix B, the way to make general decomposition of the NN potential (the Okubo-Marshak decomposition²⁵⁾) is reviewed. In Appendix C, matrix elements of the general NN potential are presented. In Appendix D, heat-kernel representation of the Green's function is presented.

§2. Non-local potential in quantum mechanics

2.1. Two-body force

To show the basic concept of the non-local potential in a finite box with the size $L \times L \times L$, we start with a non-relativistic two-body problem described by the stationary Schrödinger equation:

$$(\nabla^2 + k_n^2)\psi_n(\mathbf{r}) = 2\mu \int U(\mathbf{r}, \mathbf{r}')\psi_n(\mathbf{r}')d^3r', \quad (2.1)$$

where \mathbf{r} is the relative coordinate of the two spinless and non-relativistic particles, and k_n is related to the discrete energy eigenvalues $E_n = k_n^2/(2\mu)$ ($n = 0, 1, 2, \dots$) with μ being the reduced mass. The wave function obeys the periodic boundary condition. The non-local potential $U(\mathbf{r}, \mathbf{r}')^*$ is assumed to be energy-independent and Hermitian, $U^*(\mathbf{r}', \mathbf{r}) = U(\mathbf{r}, \mathbf{r}')$, so that the discrete energy eigenvalues E_n are real and corresponding eigenfunctions can be made orthonormal. For the scattering states (bound states) in the infinite volume, we have $E(L \rightarrow \infty) > 0$ ($E(L \rightarrow \infty) < 0$). On the other hand, negative $E_n(L)$ in the finite volume does not necessarily imply the existence of the bound state at $L \rightarrow \infty$.

We consider the potential whose spatial extension is sufficiently small in the sense that $U(\mathbf{r}, \mathbf{r}')$ is exponentially suppressed for $\{|\mathbf{r}|, |\mathbf{r}'|\} > R$ with R being smaller than $L/2$. We define the “inner region” by $\Omega_{\text{in}} = \{\mathbf{r} \in L^3 | |\mathbf{r}| < R\}$. Then, the wave function in the “outer region” $\Omega_{\text{out}} = L^3 - \Omega_{\text{in}}$ satisfies the Helmholtz equation, $(\nabla^2 + k_n^2)\psi_n(\mathbf{r}) = 0$, with the periodic boundary condition.

Let us consider the following inverse problem: Suppose we have no information about U except that it is smooth and short ranged, while we know linearly independent wave functions $\psi_n(\mathbf{r})$ and associated energy $E_n = k_n^2/(2\mu)$ in a finite box for $n \leq n_c$.**) Now, we introduce the following function:

$$K_n(\mathbf{r}) = \frac{1}{2\mu}(\nabla^2 + k_n^2)\psi_n(\mathbf{r}) = \langle \mathbf{r} | (E_n - H_0) | n \rangle, \quad (2.2)$$

where H_0 is the non-relativistic kinetic energy operator satisfying $\langle \mathbf{r} | H_0 | n \rangle =$

*) Here we use the standard term “non-local” in the sense that $U(\mathbf{r}, \mathbf{r}')$ cannot be written as $V(\mathbf{r})\delta(\mathbf{r} - \mathbf{r}')$.

**) This is more luxurious situation than the usual inverse scattering problem where only the scattering phase shifts in the outer region are available.

$\frac{1}{2\mu}\nabla^2\psi_n(\mathbf{r})$. Since $(\nabla^2 + k_n^2)$ removes the non-interacting part of the wave function, $K_n(\mathbf{r})$ is non-vanishing only in the inner region Ω_{in} irrespective of the sign of k_n^2 .

By taking into account the fact that $\psi_n(\mathbf{r}) = \langle \mathbf{r} | n \rangle$ may not be orthonormal, we introduce the norm kernel $\mathcal{N}_{nn'} \equiv \langle n | n' \rangle = \int d^3r \psi_n^*(\mathbf{r}) \psi_{n'}(\mathbf{r})$, so that the projection operator to the space spanned by the wave functions with $n \leq n_c$ reads $P(n_c) = \sum_{n,n'}^{n_c} |n\rangle \mathcal{N}_{nn'}^{-1} \langle n'| \equiv \sum_n^{n_c} P_n$. Then, an energy-independent and non-local potential can be defined as

$$U(\mathbf{r}, \mathbf{r}') = \langle \mathbf{r} | \left[\sum_n^{n_c} (E_n - H_0) P_n \right] | \mathbf{r}' \rangle = \sum_{n,n'}^{n_c} K_n(\mathbf{r}) \mathcal{N}_{nn'}^{-1} \psi_{n'}^*(\mathbf{r}'), \quad (2.3)$$

which leads to the Schrödinger equation Eq. (2.1) for $\psi_{n \leq n_c}(\mathbf{r})$. If we apply a unitary transformation A to the wave function, $\psi \rightarrow \psi' = A\psi$, the non-local potential is modified as $U \rightarrow U' = AUA^\dagger$. Such unitary transformation does not affect the observables, while it changes the spatial structure of the wave function and the non-local potential.

If E_n are all real and $\mathcal{N}_{nn'} = \delta_{nn'}$, the potential $U = \sum_n^{n_c} (E_n - H_0) P_n$ becomes a hermitian operator $\langle n | U | n' \rangle^* = \langle n' | U | n \rangle$ in the subspace $n \leq n_c$. Otherwise, the hermiticity is not obvious and should be checked case by case. In field theory discussed later, $\psi_n(\mathbf{r})$ corresponds to the equal-time Bethe-Salpeter amplitude in a finite box and E_{n_c} corresponds to the threshold energy E_{th} of inelastic channels.

In practice, the potential defined in Eq. (2.3) has limited use, because the number of states satisfying the condition $E \leq E_{\text{th}}$ is not generally large for lattice QCD in a finite box. This problem can be evaded when we focus on the low-energy scattering with E sufficiently smaller than the intrinsic scale of the system or the scale of the non-locality of the potential. In such a case, the velocity expansion of $U(\mathbf{r}, \mathbf{r}')$ in terms of its non-locality is useful:²⁶⁾ For example, a spin-independent potential with hermiticity, rotational invariance, parity symmetry, and time-reversal invariance can be expanded as

$$U(\mathbf{r}, \mathbf{r}') = V(\mathbf{r}, \mathbf{v}) \delta(\mathbf{r} - \mathbf{r}'), \quad (2.4)$$

$$V(\mathbf{r}, \mathbf{v}) = V_0(r) + \frac{1}{2} \{V_{v^2}(r), \mathbf{v}^2\} + V_{\ell^2}(r) \mathbf{L}^2 + \cdots, \quad (2.5)$$

where $\mathbf{v} = \mathbf{p}/\mu$ and $\mathbf{L} = \mathbf{r} \times \mathbf{p}$ with $\mathbf{p} = -i\nabla$. Each coefficient of the expansion is the local potential and can be determined successively by the wave functions at low energies: For example, if we have five wave functions corresponding to $E_{n=0,1,2,3,4}$, we obtain

$$(E_n - H_0) \psi_n(\mathbf{r}) = \left[V_0(r) + \frac{1}{2} \{V_{v^2}(r), \mathbf{v}^2\} + V_{\ell^2}(r) \mathbf{L}^2 \right] \psi_n(\mathbf{r}). \quad (2.6)$$

Pretending that $V_{v^2}(r)$ and $(\frac{\partial}{\partial r})^n V_{v^2}(r)$ are independent of each other, Eq. (2.6) for $n = 0, \dots, 4$ can be solved algebraically to obtain $V_0(r)$, $V_{v^2}(r)$, $\frac{\partial}{\partial r} V_{v^2}(r)$, $(\frac{\partial}{\partial r})^2 V_{v^2}(r)$ and $V_{\ell^2}(r)$. Hermiticity of the potential can be checked by the consistency among

the local potentials thus determined. Stability of the potentials against the number of wave functions introduced can be also checked.

An advantage of defining the potential from the wave functions in the “inner region” is that the effect of the periodic boundary condition is exponentially suppressed for finite range interactions: Then one can first make appropriate extrapolation of $U(\mathbf{r}, \mathbf{r}')$ or $V(\mathbf{r}, \mathbf{v})$ to $L \rightarrow \infty$, and then solve the Schrödinger equation using the extrapolated potential to calculate the observables such as the phase shifts and binding energies in the infinite volume.^{*)} This is in contrast to the approach by Lüscher¹⁵⁾ in which the wave functions in the “outer region” suffering from the boundary conditions is ingeniously utilized to probe the scattering observables. Apparently, the two approaches are the opposite sides of a same coin.

2.2. Many-body forces

For the interactions among composite particles, there are in principle many-body forces which take place in the system composed of more than two particles. The well-known example in nuclear physics is the Fujita-Miyazawa type three-body force acting among three nucleons.^{27),28)} It is phenomenologically important for the extra binding of light nuclei²⁹⁾ and for the extra repulsion in high density matter³⁰⁾ and in elastic nucleus-nucleus scatterings.³¹⁾

The method to define the two-body potential from the relative wave function discussed above can be generalized to the many-body forces. Let us illustrate the procedure by considering the three-body system of spinless and distinguishable particles with equal mass m . We consider the local potentials for both two-body and three-body forces just for simplicity. In the rest frame of the three-body system, we have

$$(E_n - H_{0r} - H_{0\rho})\psi_n(\mathbf{r}, \boldsymbol{\rho}) = \left[\sum_{i>j} V_2(\mathbf{x}_i, \mathbf{x}_j) + V_3(\mathbf{x}_1, \mathbf{x}_2, \mathbf{x}_3) \right] \psi_n(\mathbf{r}, \boldsymbol{\rho}), \quad (2.7)$$

where $\mathbf{r}(= \mathbf{x}_1 - \mathbf{x}_2)$ and $\boldsymbol{\rho}(= \mathbf{x}_3 - (\mathbf{x}_1 + \mathbf{x}_2)/2)$ are the Jacobi coordinates. $H_{0r} = -\nabla_r^2/(2\mu_r)$ and $H_{0\rho} = -\nabla_\rho^2/(2\mu_\rho)$ are the kinetic energy operator with $\mu_r(= m/2)$ and $\mu_\rho(= 2m/3)$ being the reduced masses. E_n is the total energy of the three-body system at rest. Because of the translational invariance, the two-body potential V_2 and the three-body potential V_3 are the functions of \mathbf{r} and $\boldsymbol{\rho}$.

If we know the wave function and the total energy on the left-hand side of Eq. (2.7), the three-body potential can be determined by the following procedure. We first consider the situation, $|\boldsymbol{\rho}| \gg R \gg |\mathbf{r}|$, where $V_2(\mathbf{x}_2, \mathbf{x}_3)$, $V_2(\mathbf{x}_1, \mathbf{x}_3)$ and $V_3(\mathbf{x}_1, \mathbf{x}_2, \mathbf{x}_3)$ are vanishingly small because of the assumed short-range nature of the potentials. Then, $V_2(\mathbf{x}_1, \mathbf{x}_2)$ can be determined by changing \mathbf{r} within the range $R > |\mathbf{r}|$. One can carry out similar procedure to determine $V_2(\mathbf{x}_2, \mathbf{x}_3)$ and $V_2(\mathbf{x}_1, \mathbf{x}_3)$. Alternatively, one may determine V_2 from the genuine two-body system.

Once all the two-body potentials are determined, V_3 can be extracted from the wave function in the range, $R > |\mathbf{r}|$ and $R > |\boldsymbol{\rho}|$, through the three-body

^{*)} Strictly speaking, the local potentials with higher derivatives must be treated as perturbation to keep the Schrödinger equation as a second order differential equation.

equation Eq. (2·7). It is important to note that the three-body potential is always obtained together with the two-body potential: they are closely tied through the wave function. If one makes the unitary transformation of the wave function, both V_2 and V_3 are changed simultaneously.

The above procedure can be formally generalized to the non-local potentials and to the $N(> 3)$ -particle systems with different masses and internal degrees of freedom.

§3. Non-local potential in field theory for spin 1/2 particles

3.1. Bethe-Salpeter wave function

In field theory, the best analogue of the two-particle wave function is the equal-time Bethe-Salpeter (BS) amplitude, so that we use the term “BS wave function” throughout this paper. Let us consider the following BS wave function for the 6-quark state with total energy W and the total three-momentum $\mathbf{P} = 0$ in a finite box L^3 ,

$$\Psi_{\alpha\beta}(\mathbf{r}, t) = \langle 0 | n_\beta(\mathbf{y}, t) p_\alpha(\mathbf{x}, t) | B = 2; W, \mathbf{P} = 0 \rangle \equiv \psi_{\alpha\beta}(\mathbf{r}) e^{-iWt}, \quad (3.1)$$

where the relative coordinate is denoted as $\mathbf{r} = \mathbf{x} - \mathbf{y}$. The local composite operators for the proton and the neutron are denoted by $p_\alpha(\mathbf{x}, t)$ and $n_\beta(\mathbf{y}, t)$ with spinor indices α and β . The QCD vacuum is denoted by $|0\rangle$, while the state $|B = 2; W, \mathbf{P} = 0\rangle$ is a QCD eigenstate with baryon number 2 and with the same quantum numbers as the pn system. One should keep in mind that $|B = 2; W, \mathbf{P} = 0\rangle$ is *not* a simple superposition of a product state $|p\rangle \otimes |n\rangle$, since there are complicated exchanges of quarks and gluons between the two composite particles. The stationary BS wave function $\psi(\mathbf{r})$ may be regarded as a probability amplitude in $|B = 2; W, \mathbf{P} = 0\rangle$ to have “neutron-like” three-quarks located at point \mathbf{y} and “proton-like” three-quarks located at point \mathbf{x} .

The spatial extent of the NN interaction in QCD is short ranged and is exponentially suppressed beyond the distance $R > 2$ fm. Therefore, the spatial part of the BS wave function in the “outer region” ($r > R$) satisfies the Helmholtz equation, $((W/2)^2 - \nabla^2 + m_N^2)\psi_{\alpha\beta}(\mathbf{r}) = -(\nabla^2 + k^2)\psi_{\alpha\beta}(\mathbf{r}) = 0$, up to an exponentially small correction. Here the “asymptotic momentum” k is related to the total energy W through the relation, $W = 2\sqrt{k^2 + m_N^2}$. To make a formal resemblance with the non-relativistic case, we introduce the “effective center of mass energy”, $E = k^2/(2\mu) = k^2/m_N$.¹⁵⁾ As shown in Appendix A, using the unitarity of the S -matrix, we can show that the asymptotic behaviour of the BS wave function at large r is identical to that of the scattering wave in the quantum mechanics, with the identification that the phase of the S -matrix is the scattering phase shift of the BS wave function.

Now, we apply the same logic as the quantum mechanical case in §2.1. The threshold of the pion production $E_{\text{th}} \simeq m_\pi$ is chosen to be E_{n_c} . Namely, $(\nabla^2 + k^2)\psi_{\alpha\beta,E}(\mathbf{r})$ is a function which has a support only in the inner region as long as E stays below the threshold. Thus we can define the short-ranged non-local potential

as

$$(E - H_0)\psi_{\alpha\beta,E}(\mathbf{r}) = \int U_{\alpha\beta;\gamma\delta}(\mathbf{r}, \mathbf{r}')\psi_{\gamma\delta,E}(\mathbf{r}')d^3r', \quad (3.2)$$

$$U_{\alpha\beta;\gamma\delta}(\mathbf{r}, \mathbf{r}') = \sum_{E,E'}^{E_{\text{th}}} K_{\alpha\beta,E}(\mathbf{r})\mathcal{N}_{EE'}^{-1}\psi_{\gamma\delta,E'}^*(\mathbf{r}') \quad (3.3)$$

$$= V_{\alpha\beta;\gamma\delta}(\mathbf{r}, \mathbf{v})\delta(\mathbf{r} - \mathbf{r}'), \quad (3.4)$$

where $E = k^2/m_N$ and $H_0 = -\nabla^2/m_N$. By construction, the solution of Eq. (3.2) with $U_{\alpha\beta;\gamma\delta}(\mathbf{r}, \mathbf{r}')$ extrapolated to $L \rightarrow \infty$ reproduces the correct BS wave function in the asymptotic region, and hence the phase shifts and binding energies of the two-nucleon system.

The Schrödinger type equation with the non-local potential similar to Eq. (3.2) has been derived for bosons on the basis of a diagrammatic method in Refs. 15) and 32). A slight difference is that our non-local potential has no explicit E -dependence by construction as seen in Eq. (3.3).

3.2. Interpolating operators

In Eq. (3.1), simplest interpolating operators for the neutron and the proton written in terms of the up-quark field $u(x)$ and the down-quark fields $d(x)$ would be

$$n_\beta(y) = \varepsilon_{abc}(u_a(y)C\gamma_5 d_b(y))d_{c\beta}(y), \quad (3.5)$$

$$p_\alpha(x) = \varepsilon_{abc}(u_a(x)C\gamma_5 d_b(x))u_{c\alpha}(x), \quad (3.6)$$

where $x = (\mathbf{x}, t)$, $y = (\mathbf{y}, t)$ and the color indices are denoted by a , b and c . The charge conjugation matrix in the spinor space is denoted by C .

As shown in Appendix A, local operators such as given in Eqs. (3.5) and (3.6) are most convenient for relating the BS wave function to the four-point Green's function and the scattering observables at $L \rightarrow \infty$. Closely related observation was obtained long time ago by Nishijima, Zimmermann and Hagg who derived the generalized reduction formula for local composite fields.³³⁾

In principle, one may choose any composite operators with the same quantum numbers as the nucleon to define the BS wave function.^{*)} Different operators give different BS wave functions and different NN potentials, although they lead to the same observables such as the phase shifts and binding energies. This is quite analogous to the situation in quantum mechanics that the unitary transformation of the wave function changes the structure of the potential while the observables are not modified. A theoretical advantage of our approach based on lattice QCD is that we can unambiguously trace the one-to-one correspondence between the NN potential and the interpolating operator in QCD. This is in contrast to the phenomenological NN potentials where connections to QCD operators are not attainable.

^{*)} In practice, however, we had better restrict ourselves to consider only *local* composite operators for the nucleon, since it is very difficult, although not entirely impossible, to derive the reduction formula for non-local composite operators without violating the causality of relativistic theories.

Table I. Two-nucleon asymptotic states classified by the total isospin I , the total spin (s), the orbital angular momentum (ℓ), and the total angular momentum (J) together with some examples in low partial waves.

| I | 0 | | | 1 | | |
|----------|----------|----------|----------------|----------|----------|----------------|
| s | 0 | 1 | | 0 | 1 | |
| ℓ | odd | even | | even | odd | |
| J | ℓ | ℓ | $\ell \pm 1$ | ℓ | ℓ | $\ell \pm 1$ |
| $J = 0$ | — | — | — | 1S_0 | — | 3P_0 |
| $J = 1$ | 1P_1 | — | $^3S_1, ^3D_1$ | — | 3P_1 | — |
| $J = 2$ | — | 3D_2 | — | 1D_2 | — | $^3P_2, ^3F_2$ |
| $J = 3$ | 1F_3 | — | $^3D_3, ^3G_3$ | — | 3F_3 | — |
| $J = 4$ | — | 3G_4 | — | 1G_4 | — | $^3F_4, ^3H_4$ |
| \vdots | \vdots | \vdots | \vdots | \vdots | \vdots | \vdots |

§4. General form of the NN potential

In the previous section, we illustrated the procedure to define the potential between the neutron and the proton, which has spinor indices $\alpha, \beta, \gamma, \delta$ running from 1 to 4. In order to derive the general structure of the NN potential at low energies, we restrict ourselves to consider only the upper components of these spinor indices in the following sections.

4.1. Symmetry of the two nucleon system

It is useful to classify the asymptotic two-particle states by the orbital angular momentum (ℓ), the total spin (s) and the total angular momentum (J) together with the total isospin I . Using the standard notation, $^{2s+1}\ell_J$, and taking into account constraints due to Pauli principle, we have the well-known relations given in Table I.

4.2. Okubo-Marshak decomposition

The general form of the NN potential in the two-component spinor space has been classified by Okubo and Marshak.²⁵⁾ We leave the derivation in Appendix B and recapitulate only the results here. By using the hermiticity, translational invariance in space and time, Galilei invariance, rotational invariance, parity and time-reversal invariance, fermi statistics and isospin invariance, the potential has a general decomposition

$$V = \sum_I V^I(\mathbf{r}, \mathbf{v}, \boldsymbol{\sigma}_1, \boldsymbol{\sigma}_2) P_I^T, \quad (4.1)$$

$$V^I = V_0^I + V_\sigma^I(\boldsymbol{\sigma}_1 \cdot \boldsymbol{\sigma}_2) + \frac{1}{2}\{V_T^I, S_{12}\} + V_{LS}^I \mathbf{L} \cdot \mathbf{S} + \frac{1}{2}\{V_P^I, P_{12}\} + \frac{1}{2}\{V_W^I, W_{12}\}, \quad (4.2)$$

where P_τ^I is the projection operator to the iso-singlet ($I = 0$) and iso-triplet ($I = 1$):

$$P_0^\tau = \frac{1}{4} - \boldsymbol{\tau}_1 \cdot \boldsymbol{\tau}_2, \quad P_1^\tau = \frac{3}{4} + \boldsymbol{\tau}_1 \cdot \boldsymbol{\tau}_2. \quad (4.3)$$

Also, we define

$$S_{12} = 3(\boldsymbol{\sigma}_1 \cdot \hat{\mathbf{r}})(\boldsymbol{\sigma}_2 \cdot \hat{\mathbf{r}}) - \boldsymbol{\sigma}_1 \cdot \boldsymbol{\sigma}_2, \quad (4.4)$$

$$\mathbf{S} = \frac{1}{2}(\boldsymbol{\sigma}_1 + \boldsymbol{\sigma}_2), \quad \mathbf{L} = \mathbf{r} \times \mathbf{p}, \quad (4.5)$$

$$P_{12} = (\boldsymbol{\sigma}_1 \cdot \mathbf{v})(\boldsymbol{\sigma}_2 \cdot \mathbf{v}), \quad (4.6)$$

$$W_{12} = Q_{12} - \frac{1}{3}(\boldsymbol{\sigma}_1 \cdot \boldsymbol{\sigma}_2)\mathbf{L}^2, \quad (4.7)$$

$$Q_{12} = \frac{1}{2}\{\boldsymbol{\sigma}_1 \cdot \mathbf{L}, \boldsymbol{\sigma}_2 \cdot \mathbf{L}\}, \quad (4.8)$$

with $\mathbf{v} = \mathbf{p}/\mu$. The anticommutators in Eq. (4.2) are necessary to make the potential hermitian, since S_{12}, P_{12}, W_{12} do not commute with the scalar potentials $V_A^I(\mathbf{r}^2, \mathbf{v}^2, \mathbf{L}^2)$ ($A = 0, \sigma, T, LS, P, W$).

If we keep the terms only up to the first order in \mathbf{v} , we obtain the conventional form of the potential at low energies commonly used in nuclear physics:

$$V^I = V_0^I(r) + V_\sigma^I(r)(\boldsymbol{\sigma}_1 \cdot \boldsymbol{\sigma}_2) + V_T^I(r)S_{12} + V_{LS}^I(r)\mathbf{L} \cdot \mathbf{S} + O(\mathbf{v}^2), \quad (4.9)$$

or in a more conventional notation,

$$V = V_C(r) + V_T(r)S_{12} + V_{LS}(r)\mathbf{L} \cdot \mathbf{S} + O(\mathbf{v}^2), \quad (4.10)$$

$$\begin{aligned} &= V_0(r) + V_\sigma(r)(\boldsymbol{\sigma}_1 \cdot \boldsymbol{\sigma}_2) + V_\tau(r)(\boldsymbol{\tau}_1 \cdot \boldsymbol{\tau}_2) + V_{\sigma\tau}(r)(\boldsymbol{\sigma}_1 \cdot \boldsymbol{\sigma}_2)(\boldsymbol{\tau}_1 \cdot \boldsymbol{\tau}_2) \\ &\quad + [V_{T0}(r) + V_{T\tau}(r)(\boldsymbol{\tau}_1 \cdot \boldsymbol{\tau}_2)]S_{12} \\ &\quad + [V_{LS0}(r) + V_{LS\tau}(r)(\boldsymbol{\tau}_1 \cdot \boldsymbol{\tau}_2)]\mathbf{L} \cdot \mathbf{S} + O(\mathbf{v}^2). \end{aligned} \quad (4.11)$$

The central and tensor potentials, V_C and V_T , in Eq. (4.10) are the leading-order (LO) terms of $O(\mathbf{v}^0)$ in the velocity expansion, while the spin-orbit potential, V_{LS} is the next-to-leading-order (NLO) term of $O(\mathbf{v})$.

4.3. Determination of the NN potentials

For given I , s and J , the matrix elements of the LO and NLO potentials up to $O(\mathbf{v})$ in Eq. (4.11) have the following structure (see Appendix C and also see Ref. 26)):

$$V^I(r; {}^1J_J) = V_0^I(r) + V_\sigma^I(r), \quad (4.12)$$

$$V^I(r; {}^3J_J) = V_0^I(r) - 3V_\sigma^I(r) + 2V_T^I(r) - V_{LS}^I(r), \quad (4.13)$$

$$V^I(r; {}^3(J \mp 1)_J) = \begin{pmatrix} V_{--}^I(r) & V_{-+}^I(r) \\ V_{+-}^I(r) & V_{++}^I(r) \end{pmatrix}, \quad (4.14)$$

with

$$V_{--}^I(r) = V_0^I(r) - 3V_\sigma^I(r) - \frac{2(J-1)}{2J+1}V_T^I(r) + (J-1)V_{LS}^I(r), \quad (4.15)$$

$$V_{++}^I(r) = V_0^I(r) - 3V_\sigma^I(r) - \frac{2(J+2)}{2J+1}V_T^I(r) - (J+2)V_{LS}^I(r), \quad (4.16)$$

$$V_{-+}^I(r) = V_{+-}^I(r) = 6\frac{\sqrt{J(J+1)}}{2J+1}V_T^I(r). \quad (4.17)$$

There are 8 unknown functions, $V_{0,\sigma,LS,T}^{I=0,1}$, while we have 4 (2) diagonal and 1(0) off-diagonal matrix elements at each J for $J > 0$ ($J = 0$) as seen from Table I. On the lattice, it is relatively unambiguous to extract information for $\ell = 0, 1, 2, 3 = S, P, D, F$ using the irreducible representations of the cubic group.¹⁵⁾ Then, at most 16 independent (14 diagonal and 2 off-diagonal) information as seen in Table I are obtained for 8 unknowns $V_A^I(r)$, so that each $V_A^I(r)$ can be determined in two different ways.

4.4. Long range part of the potential

In QCD with dynamical quarks, the lightest hadron is the pion. Therefore, the longest range interaction between the nucleons is dictated by the one-pion-exchange potential (OPEP). For later purpose, let us here summarize several features of OPEP with special care about its chiral behavior.

First of all, the equivalence theorem implies that the pseudo-scalar πN coupling $g_{\pi N} (\simeq 14.0)$ and the pseudo-vector coupling $f_{\pi N}$ at low energy are related through $f_{\pi N} = \frac{g_{\pi N}}{2M_N}$. This is simply obtained by kinematics. On the other hand, chiral symmetry leads to the Goldberger-Treiman (GT) relation, $\frac{g_{\pi N}}{M_N} \simeq \frac{g_A}{F_\pi}$, where $g_A (\simeq 1.27)$ is the nucleon axial-charge and $F_\pi (\simeq 93 \text{ MeV})$ is the pion decay constant.

With these relations, the OPEP reads

$$V_{\text{OPEP}}(r) = \frac{f_{\pi N}^2}{4\pi} (\boldsymbol{\tau}_1 \cdot \boldsymbol{\tau}_2) (\boldsymbol{\sigma}_1 \cdot \nabla_1) (\boldsymbol{\sigma}_2 \cdot \nabla_2) \frac{e^{-m_\pi r}}{r} \quad (4.18)$$

$$= \frac{g_{\pi N}^2}{4\pi} \left(\frac{m_\pi}{2M_N} \right)^2 \frac{(\boldsymbol{\tau}_1 \cdot \boldsymbol{\tau}_2)}{3} \left[(\boldsymbol{\sigma}_1 \cdot \boldsymbol{\sigma}_2) + S_{12} \left(1 + \frac{3}{m_\pi r} + \frac{3}{m_\pi^2 r^2} \right) \right] \frac{e^{-m_\pi r}}{r}, \quad (4.19)$$

$$= \frac{g_A^2}{4\pi} \left(\frac{m_\pi}{2F_\pi} \right)^2 \frac{(\boldsymbol{\tau}_1 \cdot \boldsymbol{\tau}_2)}{3} \left[(\boldsymbol{\sigma}_1 \cdot \boldsymbol{\sigma}_2) + S_{12} \left(1 + \frac{3}{m_\pi r} + \frac{3}{m_\pi^2 r^2} \right) \right] \frac{e^{-m_\pi r}}{r} \quad (4.20)$$

$$\xrightarrow{\text{chiral limit}} \frac{g_A^2}{16\pi F_\pi^2} (\boldsymbol{\tau}_1 \cdot \boldsymbol{\tau}_2) \frac{S_{12}}{r^3}. \quad (4.21)$$

Here we have used the equivalence theorem to obtain Eq. (4.19) from Eq. (4.18) and use the GT relation to obtain Eq. (4.20) from Eq. (4.19). g_A and F_π in Eq. (4.21) are the values in the chiral limit.

In quenched QCD without dynamical quarks, there arises a dipole ghost in the flavor-singlet channel (the η -channel in the case of two flavors) which couples to the nucleons.^{34), 35)} The η -propagator in the quenched approximation is written as

$$D_\eta(q) = \frac{i}{q^2 - m_\pi^2 + i\epsilon} + \frac{iM_0^2(q)}{(q^2 - m_\pi^2 + i\epsilon)^2}, \quad (4.22)$$

where $M_0^2(q) \equiv m_0^2 - \alpha_0 q^2$ with m_0 and α_0 being ghost parameters. The second

term is the dipole ghost corresponding to the hairpin diagram with quark-line disconnected. Then the NN potential from the η exchange reads³⁵⁾

$$V_\eta(r) = \frac{f_{\eta N}^2}{4\pi} (\boldsymbol{\sigma}_1 \cdot \nabla)(\boldsymbol{\sigma}_2 \cdot \nabla) \left[(1 - \alpha_0) + M_0^2(m_\pi) \frac{\partial}{\partial m_\pi^2} \right] \frac{e^{-m_\pi r}}{r} \quad (4.23)$$

$$\begin{aligned} &= \frac{g_{\eta N}^2}{4\pi} \left(\frac{m_\pi}{2M_N} \right)^2 \frac{(1 - \alpha_0)}{3} \left[(\boldsymbol{\sigma}_1 \cdot \boldsymbol{\sigma}_2) + S_{12} \left(1 + \frac{3}{m_\pi r} + \frac{3}{m_\pi^2 r^2} \right) \right] \frac{e^{-m_\pi r}}{r} \\ &\quad - \frac{g_{\eta N}^2}{4\pi} \left(\frac{m_\pi}{2M_N} \right)^2 \left(\frac{M_0^2(m_\pi)}{2m_\pi} \right) \frac{1}{3} \left[(\boldsymbol{\sigma}_1 \cdot \boldsymbol{\sigma}_2) \left(1 - \frac{2}{m_\pi r} \right) + S_{12} \left(1 + \frac{1}{m_\pi r} \right) \right] e^{-m_\pi r}, \end{aligned} \quad (4.24)$$

where $f_{\eta N}$ ($g_{\eta N}$) is the pseudo-vector (pseudo-scalar) coupling of the flavor-singlet η to the nucleon. Its magnitude does not necessarily be as large as the πN coupling.³⁶⁾ Note that the long range part of the potential has exponential fall-off instead of the Yukawa-type because of the dipole-term in Eq. (4.22).

Let us define a ratio \mathcal{R}_{13} between the central potential in the spin-singlet channel and that in the spin-triplet channel,

$$\mathcal{R}_{13} \equiv \frac{V_C(r; {}^1S_0)}{V_C(r; {}^3S_1)} \xrightarrow{r \rightarrow \infty} \begin{cases} +1 & \text{(one-pion-exchange),} \\ -3 & \text{(one-ghost-exchange).} \end{cases} \quad (4.25)$$

Since we have $\langle \boldsymbol{\sigma}_1 \cdot \boldsymbol{\sigma}_2 \rangle_{\text{spin-singlet}} = -3$, $\langle \boldsymbol{\sigma}_1 \cdot \boldsymbol{\sigma}_2 \rangle_{\text{spin-triplet}} = +1$ and the similar relations for the isospin, the large r behavior of \mathcal{R}_{13} has different sign and magnitude between the one-ghost-exchange and one-pion-exchange. Therefore \mathcal{R}_{13} can be used as a tool to identify the ghost contribution at large distance as will be discussed in §6.5.

§5. Central and tensor forces in lattice QCD

5.1. BS wave function on the lattice

To define the BS wave function on the lattice with the lattice spacing a and the spatial lattice volume L^3 , we start from the four-point correlator,

$$\mathcal{G}_{\alpha\beta}(\mathbf{x}, \mathbf{y}, t - t_0; J^P) = \langle 0 | n_\beta(\mathbf{y}, t) p_\alpha(\mathbf{x}, t) \overline{\mathcal{J}}_{pn}(t_0; J^P) | 0 \rangle \quad (5.1)$$

$$= \sum_{n=0}^{\infty} A_n \langle 0 | n_\beta(\mathbf{y}) p_\alpha(\mathbf{x}) | E_n \rangle e^{-E_n(t-t_0)}, \quad (5.2)$$

$$\xrightarrow{t \gg t_0} A_0 \psi_{\alpha\beta}(\mathbf{r}; J^P) e^{-E_0(t-t_0)}, \quad (5.3)$$

with the matrix element $A_n = \langle E_n | \overline{\mathcal{J}}_{pn}(0) | 0 \rangle$. The states created by the source $\overline{\mathcal{J}}_{pn}$ have the conserved quantum numbers, (J, J_z) (total angular momentum and its z -component) and P (parity). For studying the nuclear force in the $J^P = 0^+$ (1S_0) channel and the $J^P = 1^+$ (3S_1 and 3D_1) channel, we adopt a wall source located at

$t = t_0$ with the Coulomb gauge fixing only at $t = t_0$:

$$\mathcal{J}_{pn}(t_0; J^P) = P_{\beta\alpha}^{(s)} \left[p_{\alpha}^{\text{wall}}(t_0) n_{\beta}^{\text{wall}}(t_0) \right], \quad (5.4)$$

where $p_{\alpha}^{\text{wall}}(t_0)$ and $n_{\beta}^{\text{wall}}(t_0)$ are obtained by replacing the local quark fields $q(x)$ and $q(y)$ in Eqs. (3.5) and (3.6) by the wall quark fields,

$$q^{\text{wall}}(t_0) \equiv \sum_{\mathbf{x}} q(\mathbf{x}, t_0). \quad (5.5)$$

By construction, the source operator Eq. (5.4) has zero orbital angular momentum at $t = t_0$, so that states with fixed (J, J_z) are obtained by the spin projection with $(s, s_z) = (J, J_z)$, e.g. $P_{\beta\alpha}^{(s=0)} = (\sigma_2)_{\beta\alpha}$ and $P_{\beta\alpha}^{(s=1, s_z=0)} = (\sigma_1)_{\beta\alpha}$. Note that the ℓ and s are not separately conserved: Therefore, the state created by the source $\mathcal{J}_{pn}(t_0; 1^+)$ becomes a mixture of the $\ell = 0$ and $\ell = 2$ at later time t .

The BS wave function in the orbital S-state is then defined with the projection operator for the orbital angular momentum ($P^{(\ell)}$) and that for the spin ($P^{(s)}$):

$$\psi(r; {}^1S_0) = P^{(\ell=0)} P^{(s=0)} \psi(\mathbf{r}; 0^+) \equiv \frac{1}{24} \sum_{g \in O} P_{\beta\alpha}^{(s=0)} \psi_{\alpha\beta}(g^{-1}\mathbf{r}; 0^+), \quad (5.6)$$

$$\psi(r; {}^3S_1) = P^{(\ell=0)} P^{(s=1)} \psi(\mathbf{r}; 1^+) \equiv \frac{1}{24} \sum_{g \in O} P_{\beta\alpha}^{(s=1)} \psi_{\alpha\beta}(g^{-1}\mathbf{r}; 1^+). \quad (5.7)$$

Here the summation over $g \in O$ is taken for the cubic transformation group with 24 elements to project out the S-state.^{*) , **)}

5.2. Asymptotic momentum

The asymptotic momentum k for the S-states is obtained by fitting the BS wave function $\psi(\mathbf{r})$ with the Green's function in a finite and periodic box:¹⁵⁾

$$G(\mathbf{r}; k^2) = \frac{1}{L^3} \sum_{\mathbf{n} \in \mathbf{Z}^3} \frac{e^{i(2\pi/L)\mathbf{n} \cdot \mathbf{r}}}{(2\pi/L)^2 \mathbf{n}^2 - k^2}, \quad (5.8)$$

which satisfies $(\nabla^2 + k^2)G(\mathbf{r}; k^2) = -\delta_{\text{lat}}(\mathbf{r})$ with $\delta_{\text{lat}}(\mathbf{r})$ being the periodic delta-function. In the actual calculation, Eq. (5.8) is rewritten in terms of the heat kernel \mathcal{K} satisfying the heat equation, $\partial_t \mathcal{K}(t, \mathbf{r}) = \nabla^2 \mathcal{K}(t, \mathbf{r})$ with the initial condition, $\mathcal{K}(t \rightarrow 0^+, \mathbf{r}) = \delta_{\text{lat}}(\mathbf{r})$ (see Appendix D for the detail). The fits are performed outside the range of the NN interaction determined by $\nabla^2 \psi(\mathbf{r})/\psi(\mathbf{r})$.³⁷⁾

^{*)} More precisely, this projection picks up an A_1^+ state, which contains not only an $\ell = 0$ component but also the higher orbital waves with $\ell \geq 4$. Latter contributions, however, are expected to be negligible at low energy.

^{**)} Note that $P^{(\ell=0)} P^{(s=0)}$ in Eq. (5.6) is a redundant operation, since we have already prepared $J^P = 0^+$ state by the wall source $\mathcal{J}_{pn}(t_0; 0^+)$ which allows only the 1S_0 channel. Also, $P^{(s=1)}$ in Eq. (5.7) is a redundant operation, since the $J^P = 1^+$ state prepared by the wall source $\mathcal{J}_{pn}(t_0; 1^+)$ allows only the spin-triplet state.

5.3. Effective central potential at low energies

In the S-states at low energies, the effect of the velocity dependent terms in Eq. (4.11) is supposed to be small compared to the velocity independent terms, so that it is convenient to define the “effective” central potential $V_C^{\text{eff}}(r)$:²⁰⁾

$$V_C^{\text{eff}}(r) = E + \frac{1}{m_N} \frac{\nabla^2 \psi(r)}{\psi(r)}. \quad (5.9)$$

As long as we keep only the LO terms of the velocity expansion in Eq. (4.10), $V_C^{\text{eff}}(r; {}^1S_0)$ is equivalent to $V_C(r; {}^1S_0)$, while $V_C^{\text{eff}}(r; {}^3S_1)$ differs from $V_C(r; {}^3S_1)$ due to the higher order effects from the tensor potential. One can also study the validity of velocity expansion in Eq. (4.10) by calculating $V_C^{\text{eff}}(r; {}^1S_0)$ for different energies E (see §6.9).

5.4. Scattering lengths

The NN scattering lengths for the S-states can be deduced from Lüscher’s formula,^{15), 37)}

$$k \cot \delta_0(k) = \frac{2}{\sqrt{\pi}L} Z_{00}(1; q^2) = \frac{1}{a_0} + O(k^2), \quad (5.10)$$

where $Z_{00}(1; q^2)$ with $q = \frac{kL}{2\pi}$ is obtained by the analytic continuation of the generalized zeta-function $Z_{00}(s; q^2) = \frac{1}{\sqrt{4\pi}} \sum_{\mathbf{n} \in \mathbf{Z}^3} (\mathbf{n}^2 - q^2)^{-s}$ defined for $\text{Re } s > 3/2$. (See also Ref. 38) for more general considerations.) In this formula, the sign of the S-wave scattering length a_0 is defined to be positive for weak attraction.

5.5. Decomposition into central and tensor potentials

Although the tensor force at long distance is dominated by the one-pion exchange, its spatial structure at medium and short distances is not well understood theoretically nor well determined phenomenologically. Therefore, it is quite important to extract it from lattice QCD.

In the LO of the velocity expansion in Eq. (4.10), only the central potential $V_C(r)$ and the tensor potential $V_T(r)$ are relevant: The central potential acts separately on the S and D components, while the tensor potential provides a coupling between these two. Therefore, we consider a coupled-channel Schrödinger equation in the $J^P = 1^+$ channel,³⁹⁾ in which the BS wave function has both S-wave and D-wave components:

$$(H_0 + V_C(r) + V_T(r)S_{12})\psi(\mathbf{r}; 1^+) = E\psi(\mathbf{r}; 1^+). \quad (5.11)$$

The projections to the S-wave and D-wave components similar to Eq. (5.7) read

$$\mathcal{P}\psi_{\alpha\beta} \equiv P^{(\ell=0)}\psi_{\alpha\beta}(\mathbf{r}; 1^+), \quad (5.12)$$

$$\mathcal{Q}\psi_{\alpha\beta} \equiv (1 - P^{(\ell=0)})\psi_{\alpha\beta}(\mathbf{r}; 1^+). \quad (5.13)$$

Note that both $\mathcal{P}\psi_{\alpha\beta}$ and $\mathcal{Q}\psi_{\alpha\beta}$ contain additional components with $\ell \geq 4$ but they are expected to be small at low energies.

By multiplying \mathcal{P} and \mathcal{Q} to Eq. (5.11) from the left and using the fact that H_0 , $V_C(r)$ and $V_T(r)$ commute with \mathcal{P} and \mathcal{Q} , Eq. (5.11) splits into two equations,

$$H_0[\mathcal{P}\psi](\mathbf{r}) + V_C(r)[\mathcal{P}\psi](\mathbf{r}) + V_T(r)[\mathcal{P}S_{12}\psi](\mathbf{r}) = E[\mathcal{P}\psi](\mathbf{r}), \quad (5.14)$$

$$H_0[\mathcal{Q}\psi](\mathbf{r}) + V_C(r)[\mathcal{Q}\psi](\mathbf{r}) + V_T(r)[\mathcal{Q}S_{12}\psi](\mathbf{r}) = E[\mathcal{Q}\psi](\mathbf{r}), \quad (5.15)$$

where we have suppressed the spin indices, α and β , for simplicity.

By picking up $(\alpha, \beta) = (2, 1)$ component of these two equations, we arrive at

$$V_C(\mathbf{r}) = E - \frac{1}{\Delta(\mathbf{r})} ([\mathcal{Q}S_{12}\psi]_{21}(\mathbf{r})H_0[\mathcal{P}\psi]_{21}(\mathbf{r}) - [\mathcal{P}S_{12}\psi]_{21}(\mathbf{r})H_0[\mathcal{Q}\psi]_{21}(\mathbf{r})), \quad (5.16)$$

$$V_T(\mathbf{r}) = \frac{1}{\Delta(\mathbf{r})} ([\mathcal{Q}\psi]_{21}(\mathbf{r})H_0[\mathcal{P}\psi]_{21}(\mathbf{r}) - [\mathcal{P}\psi]_{21}(\mathbf{r})H_0[\mathcal{Q}\psi]_{21}(\mathbf{r})), \quad (5.17)$$

$$\Delta(\mathbf{r}) \equiv [\mathcal{P}\psi]_{21}(\mathbf{r})[\mathcal{Q}S_{12}\psi]_{21}(\mathbf{r}) - [\mathcal{Q}\psi]_{21}(\mathbf{r})[\mathcal{P}S_{12}\psi]_{21}(\mathbf{r}). \quad (5.18)$$

§6. Numerical results in quenched QCD

6.1. Setup of the lattice simulations

We employ the standard plaquette gauge action on a 32^4 lattice with the bare QCD coupling constant $\beta = 6/g^2 = 5.7$. The corresponding lattice spacing is determined as $1/a = 1.44(2)$ GeV ($a \simeq 0.137$ fm) from the ρ meson mass in the chiral limit.⁴⁰⁾ The physical size of our lattice then reads $L \simeq 4.4$ fm. As for the fermion action, we adopt the standard Wilson quark action with the hopping parameter ($\kappa = 0.1640, 0.1665$ and 0.1678), which controls the quark masses. The periodic boundary condition is imposed on the quark fields along the spatial direction, while the Dirichlet boundary condition is imposed along the temporal direction on the time-slice $t = 0$. The wall source is placed on the time-slice at $t_0/a \equiv 5$ after the Coulomb gauge fixing at $t = t_0$.

To generate the quenched gauge configurations, we adopt the heatbath algorithm and sample configurations are taken in every 200 sweeps after skipping 3000 sweeps for thermalization. The number of sampled gauge configurations N_{conf} , the pion mass m_π , the rho-meson mass m_ρ and the nucleon mass m_N are summarized in Table II. For $\kappa = 0.1678$, we have removed 28 exceptional gauge configurations from the sample.

The BS wave functions are measured at $(t - t_0)/a = 7, 6, 5$ for $\kappa = 0.1640, 0.1665, 0.1678$, respectively. These values of $t - t_0$ are determined by studying the ground state saturation in the NN potentials as discussed below. We employ the nearest neighbor representation of the discretized Laplacian as $\nabla^2 f(\mathbf{x}) \equiv \sum_{i=1}^3 \{f(\mathbf{x} + a\mathbf{n}_i) + f(\mathbf{x} - a\mathbf{n}_i)\} - 6f(\mathbf{x})$, where \mathbf{n}_i denotes the unit vector along the i -th coordinate axis. BS wave functions are fully measured for $r < 0.7$ fm, where rapid change of the NN potential is expected. Since the change is rather modest for $r > 0.7$ fm, the measurement of BS wave functions has been restricted on the coordinate axes and their nearest neighbors to reduce the computational cost.

Table II. Summary of the hopping parameter κ , the pion mass m_π , the rho-meson mass m_ρ , the nucleon mass m_N , the time-slice $(t-t_0)/a$ at which BS wave functions are extracted, the spatial-slice R/a above which the NN potentials are inactive, and the number of gauge configurations N_{conf} with exceptional configurations being removed. The lattice spacing is $a \simeq 0.137$ fm. Some numbers are updated from Tables 1 and 2 of Ref. 21).

| κ | m_π [MeV] | m_ρ [MeV] | m_N [MeV] | $(t-t_0)/a$ | R/a | N_{conf} |
|----------|---------------|----------------|-------------|-------------|-------|-------------------|
| 0.1640 | 731.1(4) | 990.3(13) | 1558.4(63) | 7 | 11 | 1000 |
| 0.1665 | 529.0(4) | 894.3(28) | 1333.8(82) | 6 | 11 | 2000 |
| 0.1678 | 379.7(9) | 837.9(21) | 1196.6(83) | 5 | 12 | 2021 |

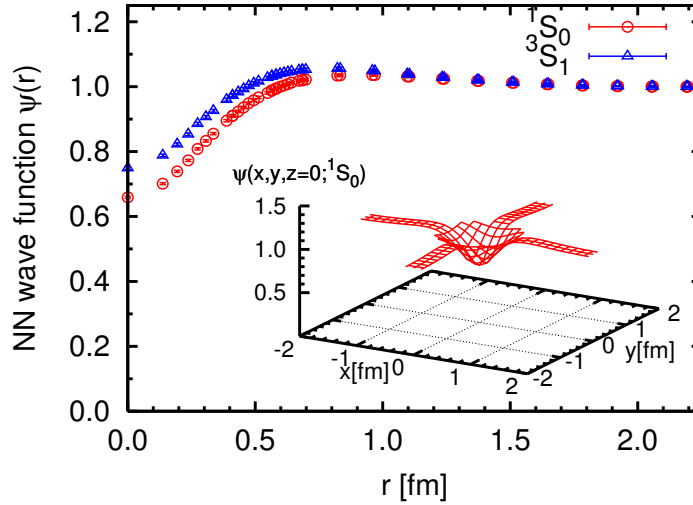


Fig. 1. The NN wave functions in 1S_0 and 3S_1 channels for $m_\pi = 529$ MeV ($\kappa = 0.1665$). The inset is a three-dimensional plot of the wave function $\psi(x, y, z = 0; ^1S_0)$.

6.2. BS wave functions in the S-state

Figure 1 shows the BS wave functions in 1S_0 and 3S_1 channels for $\kappa = 0.1665$. The wave functions are normalized to be 1 at the largest spatial point $r = 2.192$ fm.

Figure 2(a,b) show the fitting of the wave function in the interval $R/a \leq r/a \leq 16$ using Eq. (5·8). This leads to the values of the effective energy $E \equiv k^2/m_N$ in Table II. The value of R is determined from the ground state saturation of the potential as discussed below.

6.3. Effective central potential

Shown in Fig. 3 are the reconstructed effective central potentials in the 1S_0 and 3S_1 channels for $\kappa = 0.1665$ with the formula Eq. (5·9). The overall structures of the potentials are similar to the known phenomenological NN potentials discussed in §1, namely the repulsive core at short distance surrounded by the attractive well at medium and long distances. From this figure, we find that the interaction between the nucleons is well switched off for $r > 1.5$ fm, so that we chose $R/a = 11$ (for $m_\pi = 731, 529$ MeV) and $R/a = 12$ (for $m_\pi = 380$ MeV) as given in Table II. In

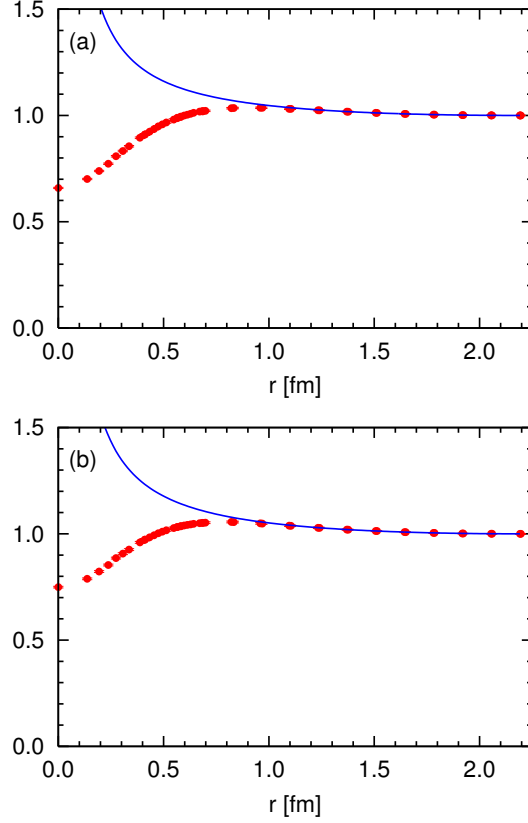


Fig. 2. (a) The fit of the NN wave functions for $m_\pi = 529$ MeV in the 1S_0 channel using the Green's function in the fit range $11 \leq r/a \leq 16$. (b) Similar fit for the NN wave functions in the 3S_1 channel.

both cases, the condition $R < L/2 = 2.2$ fm is satisfied.

To check the stability of these potentials against the time-slice adopted to define the BS wave functions, we plot the t -dependence of the 1S_0 potential for several different values of r as shown in Fig. 4 for $m_\pi = 529$ MeV: In this case, choosing $(t - t_0)/a = 6$ to extract $V_C(r)$ would be good enough to assure the stability within the statistical errors. The time-slices chosen for other cases by the same procedure are given in Table II.

6.4. Quark mass dependence of the central potential

In Fig. 5, we compare the NN central potentials in the 1S_0 channel for three different quark masses. As the quark mass decreases, the repulsive core at short distance and the attractive well at medium distance are enhanced simultaneously. This feature can be also seen in Fig. 6(a) where $r^2 V_C(r)$, which appears in the quantum mechanical matrix elements, is plotted. To study the relative magnitude of the repulsion and the attraction, we define the following volume integrals of the

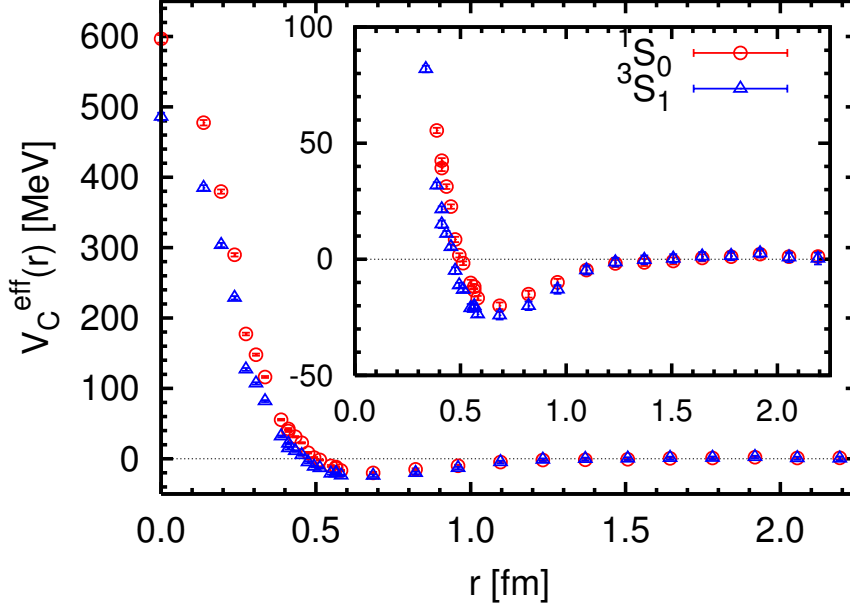


Fig. 3. The effective central potentials in the 1S_0 channel and in the 3S_1 channel for $m_\pi = 529$ MeV.

potential and plot them in Fig. 6(b):

$$I_1 = \int_0^{r_0} r^2 V_C(r) dr, \quad I_2 = \int_{r_0}^{r_1} r^2 V_C(r) dr. \quad (6.1)$$

Here r_0 (~ 0.5 fm) is the first nodal point where $r^2 V_C(r)$ changes sign from positive to negative, and r_1 is the point at which $r^2 V_C(r)$ becomes essentially zero within the statistical errors. The error bars in Fig. 6(b) reflect the uncertainties of $r_{0,1}$ as well as those from the spline curve fit of the data. The comparison of I_1 , I_2 and $I_1 + I_2$ implies that (i) both repulsion and attraction increase in magnitude as quark mass decreases, and (ii) there is a large cancellation between the repulsion and attraction, and (iii) there is a net attraction increasing as the quark mass decreases.

6.5. Dipole ghost in the central potential

To check if there is an evidence of the exponential tail from the dipole ghost in the long range part of the effective central potentials, the ratio \mathcal{R}_{13} given by Eq. (4.25) is plotted in Fig. 7 as a function of r for the lightest quark mass, $m_\pi = 380$ MeV. Within the statistical errors, there is no sign that $\mathcal{R}_{13} \rightarrow -3$ for $r > 1$ fm, so that possible ghost contamination is small in our results with relatively heavy quark masses. The figure also shows that \mathcal{R}_{13} is rather close to +1 for $r > 0.7$ fm. This does not necessary implies that the OPEP is seen: as long as there are spin-isospin independent attraction such as originating from the two-pion-exchange potential, it also leads to $\mathcal{R}_{13} \simeq 1$.

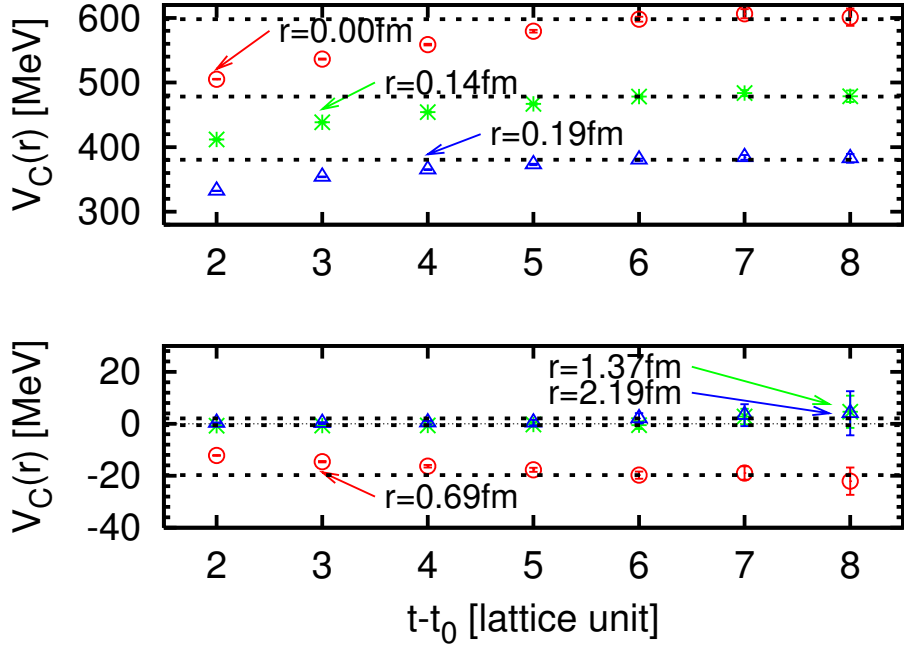


Fig. 4. The t -dependence of the potential at $r = 0, 0.14, 0.19, 1.37, 2.19, 0.69$ fm from top to bottom for the 1S_0 channel at $m_\pi = 529$ MeV.

Table III. Effective center of mass energies $E = k^2/m_N$ obtained from the asymptotic momenta for different quark mass. a_0 's are the associated scattering lengths obtained from Lüscher's formula Eq. (5.10).

| m_π [MeV] | $E(^1S_0)$ [MeV] | $E(^3S_1)$ [MeV] | $a_0(^1S_0)$ [fm] | $a_0(^3S_1)$ [fm] |
|---------------|------------------|------------------|-------------------|-------------------|
| 731.1(4) | -0.400(83) | -0.480(97) | 0.115(26) | 0.141(31) |
| 529.0(4) | -0.509(94) | -0.560(114) | 0.126(25) | 0.140(31) |
| 379.7(9) | -0.675(264) | -0.968(374) | 0.153(66) | 0.230(101) |

6.6. NN scattering lengths

As we found in Fig. 6, the central potential multiplied by r^2 shows a net attraction as a result of the large cancellation between the short range repulsion and the medium range attraction. This attractive nature of the potential can be quantified by the scattering length a_0 defined from Lüscher's formula, Eq. (5.10), together with the asymptotic momentum k obtained from Eq. (5.8).*)

The results of a_0 are summarized in the last two columns in Table III where $O(k^2)$ correction on the right-hand side of Eq. (5.10) is assumed to be small for the present energy $E = k^2/m_N$. In Fig. 8, the scattering lengths for 1S_0 and 3S_1 channels are shown as a function of m_π^2 . Although there is a small attraction which increases as m_π decreases in both channels, the absolute magnitudes of a_0 are much

*) If the net interaction is small in the infinite volume limit, the volume integral of the potential and the scattering length are related in the Born approximation as, $a_0^{\text{weak-coupling}} \simeq -m_N \int V_C(r) r^2 dr$.

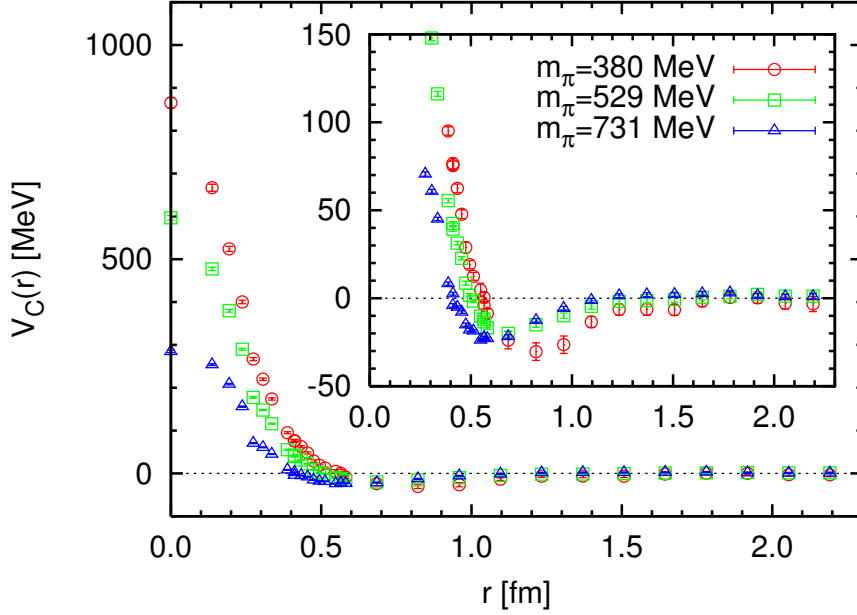


Fig. 5. The central potentials in the 1S_0 channel for three different quark masses.

smaller than the experimental values at the physical point: $a_0^{(\text{exp})}(^1S_0) \sim 20$ fm and $a_0^{(\text{exp})}(^3S_1) \sim -5$ fm at $m_\pi^2 = 0.018$ GeV 2 .

The above discrepancy is partly attributed to the heavy quark masses employed in our simulations: If we can get closer to the physical quark mass in full QCD simulations, there should arise the “unitary region” where the NN scattering length becomes singular and changes sign. This was first noted in clear terms by Kuramashi²³⁾ and was later elaborated in Refs. 19) and 41) by using chiral perturbation theory. The singularity is associated with the formation of the di-nucleon bound state, so that the NN scattering length becomes a non-linear function of the quark mass in the unitary region. As suggested in Ref. 23) by using the one-boson-exchange model with the quark-mass dependence of the hadron masses taken from the lattice QCD data, the size of the unitary region could be narrow, which implies that the scattering lengths at the heavy quark masses adopted in our simulation can be as small as the values in Fig. 8.

Unlike the scattering length, the NN potential would not have singular behavior in the unitary region as expected from the well-known quantum mechanical examples such as the low-energy scattering between ultracold atoms. Also, the effective range parameter would be a rather smooth function of the quark mass. To check these points in QCD, it is important to study the NN potential, the scattering length and the effective range simultaneously in the full QCD simulations which allow us to approach small quark masses without quenched artifact. Studies along this direction is now underway³⁹⁾ and will be reported elsewhere.

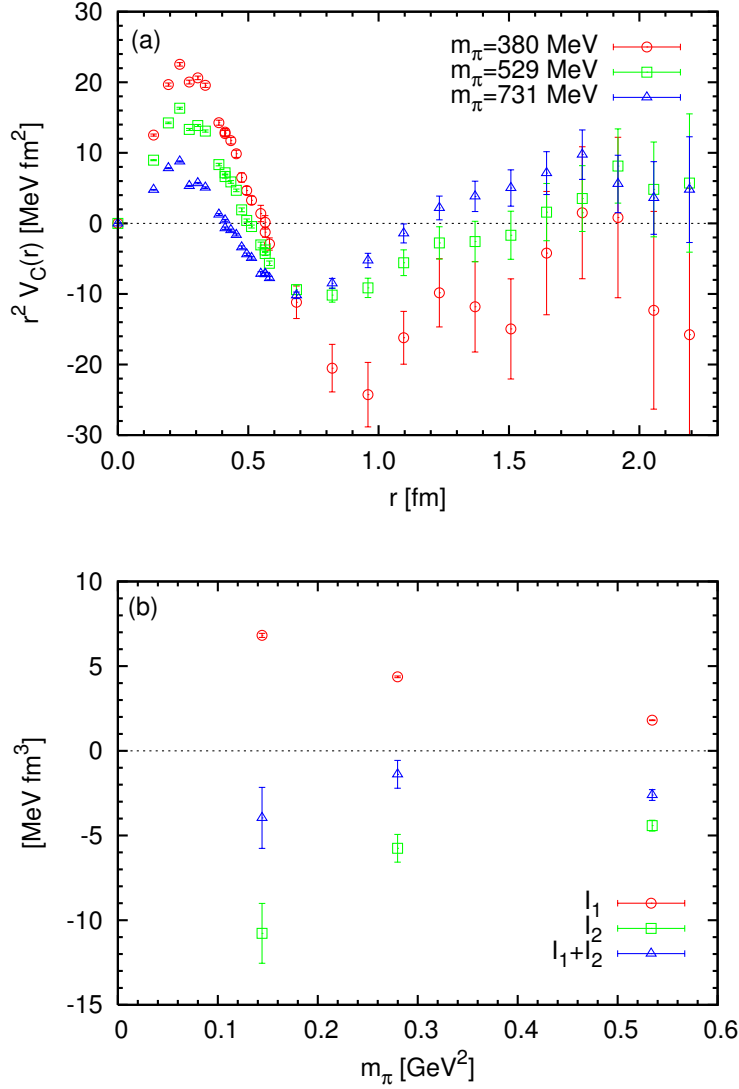


Fig. 6. (a) The central potentials with r^2 multiplied in the 1S_0 channel for three different quark masses. (b) Comparison of the attractive part and repulsive part of the potential in terms of the volume integral in the 1S_0 channel.

6.7. BS wave function in the D-state

In Fig. 9(a), we show the 3S_1 and 3D_1 components of the BS wave functions obtained from the $J^P = 1^+, J_z = M = 0$ state for $m_\pi \simeq 529 \text{ MeV}$, according to the procedure given in §5.5. To reduce the computational cost, the points are restricted on the coordinate axes and their nearest neighbors for $r > 0.7 \text{ fm}$, whereas all points are calculated for $r < 0.7 \text{ fm}$.

Note that the 3D_1 wave function as a function of r is multivalued due to its angular dependence. Since $(\alpha, \beta) = (2, 1)$ spin component of the D-state wave function for $J^P = 1^+, M = 0$ is proportional to the spherical harmonics $Y_{20}(\theta, \phi) \propto 3 \cos^2 \theta - 1$,

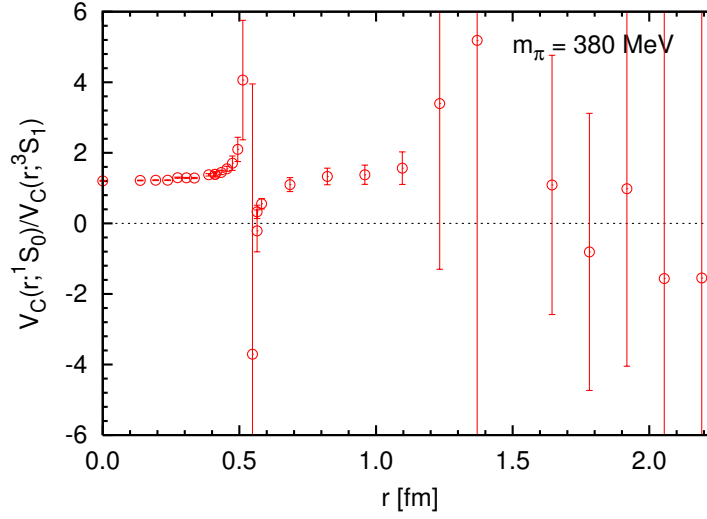


Fig. 7. The ratio of the central potentials defined in Eq. (4.25) for the lightest quark mass, $m_\pi = 380$ MeV.

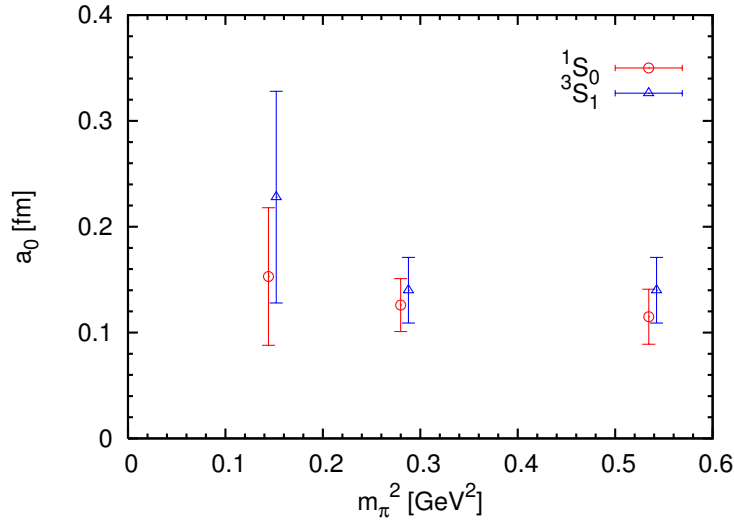


Fig. 8. Scattering length a_0 in the 1S_0 and 3S_1 channels for three different quark masses obtained in the quenched QCD simulations.

it is a good consistency test to check if the multivaluedness can be absorbed by this angular dependence. Shown in Fig. 9(b) are the same BS wave functions as Fig. 9(a) with the angular dependence in the D-state assumed to have this spherical harmonics form. It is clear that the multivaluedness is nicely removed, and thus it is certain that we indeed extracted the D-state wave function on the lattice.

6.8. Tensor force and its quark mass dependence

Shown in Fig. 10 are the central potential $V_C(r)$ and tensor potential $V_T(r)$ together with effective central potential $V_C^{\text{eff}}(r)$ in the 3S_1 channel. (As mentioned

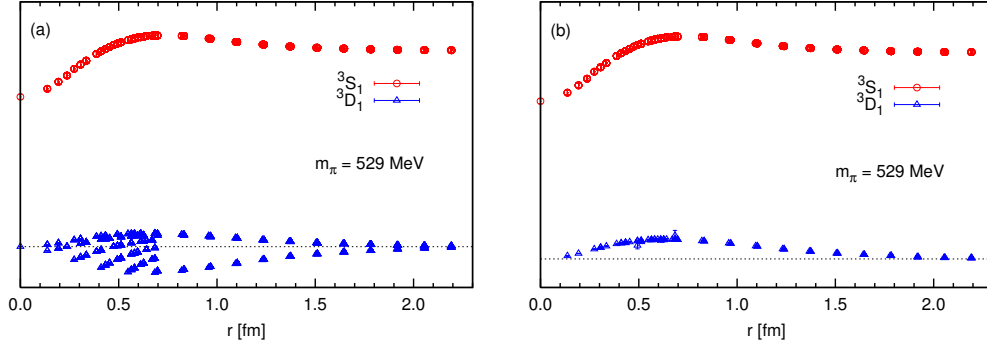


Fig. 9. (a) $(\alpha, \beta) = (2, 1)$ components of the S-state and the D-state BS wave functions projected out from a single state with $J^P = 1^+, M = 0$. (b) The same data with the spherical harmonics components are removed in the D-state.

before, we consider only the LO terms of the velocity expansion here by assuming that the NLO term (the spin-orbit potential) and higher order terms are negligible at this low energy.)

Note that $V_C^{\text{eff}}(r)$ contains the effect of $V_T(r)$ implicitly as higher order effects through the process such as $^3S_1 \rightarrow ^3D_1 \rightarrow ^3S_1$. In the real world, $V_C^{\text{eff}}(r)$ is expected to acquire sufficient attraction from the tensor force. This is the reason why bound deuteron exists in the 3S_1 channel while the bound dineutron does not exist in the 1S_0 channel. Now, we see from Fig. 10 that the difference between $V_C(r)$ and $V_C^{\text{eff}}(r)$ is still small in our quenched simulations due to relatively large quark masses. This is also consistent with the results of the small scattering length shown in Fig. 8.

The tensor potentials $V_T(r)$ in Fig. 10 are negative for the whole range of r within statistical errors and have a minimum at short distance around 0.4 fm. If the tensor force receives significant contribution from the one-pion exchange as expected from the meson theory, $V_T(r)$ would be rather sensitive to the change of the quark mass. As shown in Fig. 11, it is indeed the case: Attraction of $V_T(r)$ is substantially enhanced as the quark mass decreases. A phenomenological fit of the tensor force taking into account this physics will be given later.

As discussed in §6.5, the ratio \mathcal{R}_{13} of the effective central potentials in the 1S_0 and 3S_1 channels is close to unity for $r > 0.7$ fm so that we do not see evidence of the dipole ghost (quenched artifact) in the long range part of the potential with our relatively heavy quark masses. However, this does not necessary imply that the OPEP is seen in the effective central potentials: If the OPEP dominates at long distances, Eq. (4.19) immediately implies that the magnitude of the tensor potential is always larger than the central potential at long distances. Since this is not seen in Fig. 10 within the statistical errors, it is unlikely to interpret the attraction of $V_C^{\text{eff}}(r)$ at $0.5 \text{ fm} < r < 1 \text{ fm}$ as the evidence of OPEP.

A technical comment is in order here. Since we use the $(\alpha, \beta) = (2, 1)$ spin component of Eq. (5.16), the second equation vanishes at $\mathbf{r} \propto (\pm 1, \pm 1, \pm 1)$. This is because the spin (2, 1) component of the D-state wave function is proportional to $Y_{20}(\theta, \phi) \propto 3 \cos^2 \theta - 1$ which vanishes at $\mathbf{r} \propto (\pm 1, \pm 1, \pm 1)$. Although these points

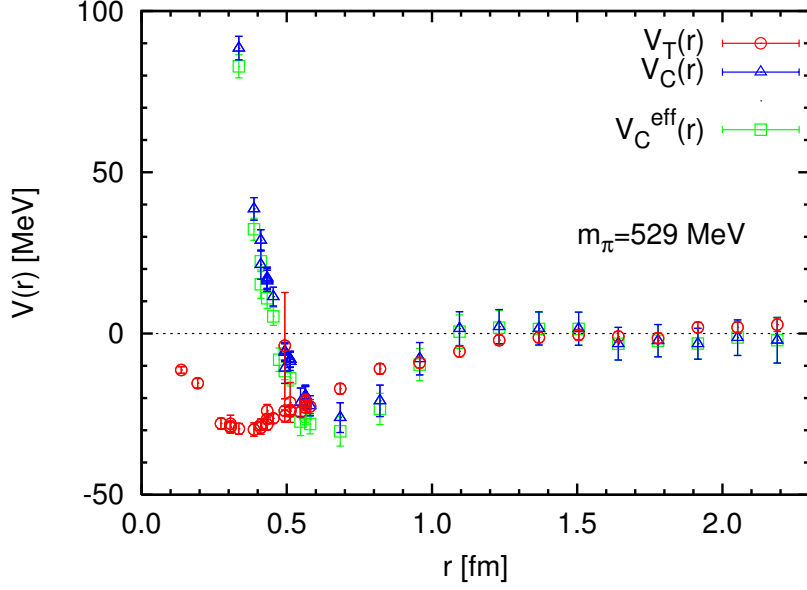


Fig. 10. The central potential $V_C(r)$ and the tensor potential $V_T(r)$ obtained from the $J^P = 1^+$ BS wave function at $m_\pi = 529$ MeV.

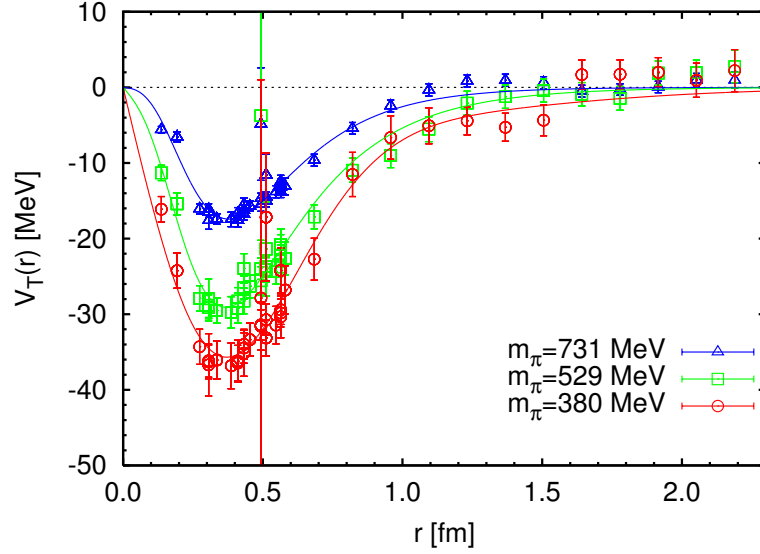


Fig. 11. Quark mass dependence of tensor force. The lines are the four-parameter fit using the one- ρ -exchange + one-pion-exchange with Gaussian form factors.

are removed from our plots, statistical error is accumulated in the neighborhood of these points. (For instance, see the points at $r \simeq 0.5$ fm in Figs. 10 and 11.) A resolution of this problem by combining the data with other spin components will be reported in the future publication.

The central and tensor potentials obtained from lattice QCD are given at dis-

crete data points. For practical applications to nuclear physics, it is more useful to parametrize the lattice results by known functions. We have tried such a fit for $V_T(r)$ under the assumption of the one- ρ -exchange + one-pion-exchange with Gaussian form factors:

$$V_T(r) = b_1(1 - e^{-b_2 r^2})^2 \left(1 + \frac{3}{m_\rho r} + \frac{3}{(m_\rho r)^2}\right) \frac{e^{-m_\rho r}}{r} + b_3(1 - e^{-b_4 r^2})^2 \left(1 + \frac{3}{m_\pi r} + \frac{3}{(m_\pi r)^2}\right) \frac{e^{-m_\pi r}}{r}, \quad (6.2)$$

where, $b_{1,2,3,4}$ are the fitting parameters while m_ρ (m_π) is taken to be the ρ -meson mass (the pion mass) calculated for each quark mass. At this moment, it is hasty to extract physical quantities from the fit such as the meson-nucleon coupling constants: Nevertheless, it may be worth mentioning that the pion-nucleon coupling constant extracted from the parameter b_3 in the case of the lightest pion mass ($m_\pi = 380$ MeV) reads $g_{\pi N}^2/(4\pi) = 12.1 \pm 2.7$ which is encouragingly close to the empirical value. We have tried similar fits for the central potential with the phenomenological repulsive core with a Gaussian form and the meson-exchange potential with form-factors: The results are still not stable enough due to the statistical errors of the lattice data.

6.9. Velocity dependence of the potential

So far we have considered the potential determined from the lattice data taken almost at zero effective energy $E \simeq 0$ MeV (see Table III). If the local potential determined from the other energies has different spatial structure, it is an indication that there are velocity dependent terms as discussed in §2.1.

A lattice QCD analysis on the velocity dependence has been recently carried out by changing the spatial boundary condition of the quark field from the periodic one to the anti-periodic one, so that the effective center of mass energy is increased to $E \sim 3(\pi/L)^2/m_N \sim 50$ MeV.⁴²⁾ The result shows that the central and tensor potentials do not show modifications for every r within the statistical errors: Namely, the non-locality of the potential with our choice of the interpolating operator is small and the potentials shown in the present paper can be used in the energy region at least up to $E \sim 50$ MeV without significant modifications.*) Detailed account of the above result is beyond the scope of this paper, and will be reported elsewhere.

§7. Summary and concluding remarks

In this paper, we have discussed the basic notion of the nucleon-nucleon potential and its field-theoretical derivation from the equal-time Bethe-Salpeter wave function in QCD. By construction, the non-local potential defined through the projection of the wave function to the interaction region (the inner region) correctly reproduces

*) An investigation based on integrable models suggests that potentials derived from the BS wave functions with local operators in these models are slowly varying functions of energy (velocity).⁴³⁾

the asymptotic form of the wave function in the region beyond the range of the nuclear force (the outer region). Thus the observables such as the phase shifts and the binding energies can be calculated after extrapolating the potential to the infinite volume limit. Non-locality of the potential can be taken into account successively by making its velocity expansion, which introduces the velocity-dependent local potentials. The leading-order terms of such velocity expansion for the nucleon-nucleon interaction are the central and the tensor potentials.

As an exploratory study to test how this formulation works, we have carried out quenched lattice QCD simulations of the two-nucleon system in a spatial box of the size $(4.4 \text{ fm})^3$ with the quark masses corresponding to $m_\pi = 380, 529, 731 \text{ MeV}$. We found that the NN potential calculated on the lattice at low energy shows all the characteristic features expected from the empirical NN potentials obtained from the experimental NN phase shifts, namely the attractive well at long and medium distances and the repulsive core at short distance for the central potential. As for the tensor potential obtained from the coupled channel treatment of the 3S_1 -state and the 3D_1 -state in the BS wave functions on the lattice, we found appreciable attraction at long and medium distances and a moderate repulsion at short distance.

As the quark mass decreases, the repulsive core and attractive well in the central potential, and the attractive well in the tensor potential tend to be enhanced. Also, we found net attraction in both 1S_0 and 3S_1 channels after the cancellation of the repulsive core and the attractive well. The absolute magnitudes of the scattering lengths are still much smaller than the physical values due to the large quark mass in our simulation. Phenomenological fit of the tensor potential strongly suggests the existence of the one-pion-exchange contribution in its long range part.

There are a number of directions to be investigated on the basis of our approach as listed below:

1. Determination of the velocity dependence is important in deriving the NN potentials which can be used for the wide range of scattering energies. Studies along this line using the anti-periodic boundary condition in the spatial direction has been already started⁴²⁾ as mentioned in §6.9.
2. To derive the realistic NN potentials on the lattice, it is necessary to carry out full QCD simulations with dynamical quarks. Studies along this line with the use of the (2+1)-flavor QCD configurations with the Wilson fermion generated by PACS-CS Collaboration⁴⁵⁾ is currently under way.³⁹⁾
3. The hyperon-nucleon (YN) and hyperon-hyperon (YY) potentials are essential for understanding the properties of hyper nuclei and the hyperonic matter inside the neutron stars. However, the experimental scattering data are very limited due to the short life-time of hyperons. On the other hand, the NN , YN and YY interactions on the lattice can be treated in the same manner by changing only the quark flavors. Recently, the ΞN potential in quenched QCD²⁴⁾ and the ΛN potential in quenched and full QCD⁴⁴⁾ are examined as a first step toward systematic derivation of the hyperon potentials.
4. The three-nucleon force is thought to play important roles in nuclear structures and in the equation of state of high density matter as mentioned in §2.2. Since the experimental information is scarce, simulations of the three nucleons on

the lattice combined with the method proposed in §2.2 may lead to the first principle determination of the three-nucleon potential in the near future.

If it turns out that the program described in this paper indeed works in full QCD with realistic quark masses, it would be the promising first step toward the understanding of atomic nuclei and neutron stars from the fundamental law of the strong interaction, the quantum chromodynamics.

Acknowledgements

The authors thank T. Doi, E. Hiyama, T. Inoue, Y. Ikeda, N. Ishizuka, A. Jackson, K. Murano, H. Nemura, S. Nishizaki, M. Oka, T. Otsuka, K. Sasaki, S. Sasaki, T. Takatsuka, R. Tamagaki, K. Yabana, Y. Yamamoto and W. Weise for useful discussions and comments. This research was supported in part by the Grant-in-Aid of MEXT (Nos. 15540254, 18540253, 19540261, 20340047) and by a Grant-in-Aid for Specially Promoted Research (No. 13002001) and by Grant-in-Aid for Scientific Research on Innovative Areas (No. 2004: 20105001, 20105003). Our simulations have been performed with IBM Blue Gene/L at KEK under a support of its Large Scale Simulation Program, No. 18 and No. 06-21 (FY2006), No. 07-07 (FY2007), No. 08-19 (FY2008) and No. 09-23 (FY2009).

Appendix A

—— Bethe-Salpeter Wave Function and Its Asymptotic Behaviour ——

In this appendix we derive the behaviour of the Bethe-Salpeter (BS) wave function at large r , only using the properties of quantum field theories.

A.1. Unitarity of S -matrix and structure of T -matrix

We first determine the structure of the NN scattering T -matrix below the pion-production threshold. Due to the unitarity of the S -matrix. $S^\dagger S = 1$ with $S = 1 + iT$, we obtain

$$\langle f|T|i\rangle - \langle f|T^\dagger|i\rangle = i \sum_n \langle f|T^\dagger|n\rangle \langle n|T|i\rangle. \quad (\text{A}\cdot 1)$$

In the case of NN scattering in the center of mass frame such that $(k_a, s_a) + (k_b, s_b) \rightarrow (k_c, s_c) + (k_d, s_d)$ where $k_a = (\varepsilon_k, \mathbf{k})$, $k_b = (\varepsilon_k, -\mathbf{k})$ and $k_c = (\varepsilon_p, \mathbf{p})$, $k_d = (\varepsilon_p, -\mathbf{p})$ with $\varepsilon_k = \sqrt{\mathbf{k}^2 + m_N^2}$ and $\varepsilon_p = \sqrt{\mathbf{p}^2 + m_N^2}$, we write

$$\text{in} \langle p_c, s_c, p_d, s_d | T | p_a, s_a, p_b, s_b \rangle_{\text{in}} = (2\pi)^4 \delta^{(4)}(p_a + p_b - p_c - p_d) T(\mathbf{p}, s_c, s_d; \mathbf{k}, s_a, s_b). \quad (\text{A}\cdot 2)$$

Here $s_i = \pm 1/2$ is a helicity of each nucleon, and $k = |\mathbf{k}| = |\mathbf{p}|$ in the center of mass frame. Below the pion production threshold such that $2\sqrt{k^2 + m_N^2} < 2m_N + m_\pi$, the sum over intermediate states n in Eq. (A.1) can be restricted to the NN states

due to energy-momentum conservations as

$$\sum_n |n\rangle\langle n| = \sum_{s_1, s_2} \int \frac{d^3 p_1}{(2\pi)^3 2\varepsilon_{p_1}} \frac{d^3 p_2}{(2\pi)^3 2\varepsilon_{p_2}} |p_1, s_1, p_2, s_2\rangle\langle p_1, s_1, p_2, s_2|. \quad (\text{A}\cdot 3)$$

This leads to

$$\begin{aligned} & T(\mathbf{p}, s_c, s_d; \mathbf{k}, s_a, s_b) - T^\dagger(\mathbf{p}, s_c, s_d; \mathbf{k}, s_a, s_b) \\ &= i \sum_{s_1, s_2} \frac{k}{32\pi^2 \varepsilon_k} \int d\Omega_q T^\dagger(\mathbf{p}, s_c, s_d; \mathbf{q}, s_1, s_2) T(\mathbf{q}, s_1, s_2; \mathbf{k}, s_a, s_b), \end{aligned} \quad (\text{A}\cdot 4)$$

where $|\mathbf{q}| = k$ and Ω_q is the solid angle of vector \mathbf{q} . Using the angular momentum basis,⁴⁶⁾

$$T(\mathbf{p}, s_c, s_d; \mathbf{k}, s_a, s_b) = 4\pi \sum_{J, M} \frac{2J+1}{4\pi} \langle s_c, s_d | T^J(k) | s_a, s_b \rangle (D^J)^\dagger_{s'M}(\Omega_p) D^J_{Ms}(\Omega_k), \quad (\text{A}\cdot 5)$$

with $s = s_a - s_b$ and $s' = s_c - s_d$, we obtain

$$T^J(k) - [T^J]^\dagger(k) = i \frac{k}{8\pi \varepsilon_k} [T^J]^\dagger(k) T^J(k). \quad (\text{A}\cdot 6)$$

Here T^J is considered as a 4×4 matrix and the Wigner D -matrix D^J is defined by

$$D^J_{M\lambda}(\Omega) = e^{-iM\alpha} d^J_{M\lambda}(\beta) e^{+i\lambda\alpha}, \quad (\text{A}\cdot 7)$$

where the solid angle is denoted as $d\Omega = \sin\beta d\beta d\alpha$ and $d^J_{M\lambda}(\beta)$ is the Wigner d -matrix. The normalization of the D -matrix is given by

$$\int d\Omega (D^J)^\dagger_{\lambda M}(\Omega) D^J_{M'\lambda}(\Omega) = \frac{4\pi}{2J+1} \delta^{JJ'} \delta_{MM'}, \quad (\text{A}\cdot 8)$$

where no summation is taken for λ . For the NN scattering, with new helicity basis such that $|+\frac{1}{2}, +\frac{1}{2}\rangle \pm |-\frac{1}{2}, -\frac{1}{2}\rangle$ and $|+\frac{1}{2}, -\frac{1}{2}\rangle \pm |-\frac{1}{2}, +\frac{1}{2}\rangle$, T^J is decomposed into two 1×1 submatrices and one 2×2 submatrix as⁴⁶⁾

$$T^J = \begin{pmatrix} T^J_{\ell=J, s=0} & 0 & 0_{1 \times 2} \\ 0 & T^J_{\ell=J, s=1} & 0_{1 \times 2} \\ 0_{2 \times 1} & 0_{2 \times 1} & T^J_{\ell=J \mp 1, s=1} \end{pmatrix}. \quad (\text{A}\cdot 9)$$

The unitarity condition then gives

$$T^J_{\ell=J, s} = \hat{T}_{Js}, \quad T^J_{\ell=J \mp 1, s=1} = O(k) \begin{pmatrix} \hat{T}_{J-1, 1} & 0 \\ 0 & \hat{T}_{J+1, 1} \end{pmatrix} O^{-1}(k), \quad (\text{A}\cdot 10)$$

with

$$\hat{T}_{\ell s} = \frac{16\pi \varepsilon_k}{k} e^{i\delta_{\ell s}(k)} \sin \delta_{\ell s}(k), \quad O(k) = \begin{pmatrix} \cos \varepsilon_J(k) & -\sin \varepsilon_J(k) \\ \sin \varepsilon_J(k) & \cos \varepsilon_J(k) \end{pmatrix}, \quad (\text{A}\cdot 11)$$

where $\delta_{\ell s}(k)$ is the scattering phase shift, whereas $\varepsilon_J(k)$ is the mixing angle between $\ell = J \pm 1$. They correspond to the standard Blatt-Biedenharn eigenphase and mixing angle.

A.2. BS amplitude and half off-shell T -matrix

Let us now consider the Bethe-Salpeter (BS) amplitude for the proton and the neutron, defined by

$$\Psi_{\alpha\beta}(x, y) = \langle 0 | T \{ n_\beta(y) p_\alpha(x) \} | p(\mathbf{q}, s) n(\mathbf{q}', s') \rangle_{\text{in}}, \quad (\text{A}\cdot 12)$$

where T represents the time-ordered product. The spatial momentum and the helicity for the incoming proton and those for the neutron are denoted by (\mathbf{q}, s) and (\mathbf{q}', s') , respectively. The single nucleon state is normalized covariantly, $\langle B_i(\mathbf{q}, s) | B_j(\mathbf{q}', s') \rangle = 2\varepsilon_q (2\pi)^3 \delta_{ij} \delta_{ss'} \delta^3(\mathbf{q} - \mathbf{q}')$ where $B_1 = p$ (proton) and $B_2 = n$ (neutron).

The fields, $n_\beta(y)$ and $p_\alpha(x)$, are the local composite operators for the neutron and the proton whose explicit forms are irrelevant for the following derivation. One of the advantages to use local operators is that the standard reduction formula can be generalized without much modification as shown by Nishijima, Zimmermann and Haag (NZH).³³⁾ In particular, one can define in and out composite fields, $n_{\text{in(out)}}(x)$ and $p_{\text{in(out)}}(x)$, in a similar way as the elementary field through the Yang-Feldman equation as³³⁾

$$\sqrt{Z} N_{\text{in(out)}}(x) = N(x) - \int S_{\text{ret(adv)}}(x - x'; m) J(x') d^4x, \quad (\text{A}\cdot 13)$$

where N takes either n or p , $S_{\text{ret(adv)}}$ denotes the retarded (advanced) Green's function in the free space with the mass $m = m_N$, and the “source” is $J(x) \equiv (i\cancel{\partial}_x - m)N(x)$. The wave function renormalization constant Z is defined as $\sqrt{Z} u_\alpha(\mathbf{p}, s) = \langle 0 | N_\alpha(0) | B(\mathbf{p}, s) \rangle$, where we have the following normalization of the Dirac spinors:

$$\sum_\alpha u_\alpha^\dagger(\mathbf{p}, s) u_\alpha(\mathbf{p}, s') = \sum_\alpha v_\alpha^\dagger(\mathbf{p}, s) v_\alpha(\mathbf{p}, s') = 2\varepsilon_p \delta_{ss'}, \quad (\text{A}\cdot 14)$$

$$\sum_s u_\alpha(\mathbf{p}, s) \bar{u}_\beta(\mathbf{p}, s) = (\cancel{p} + m)_{\alpha\beta}, \quad \sum_s v_\alpha(\mathbf{p}, s) \bar{v}_\beta(\mathbf{p}, s) = (\cancel{p} - m)_{\alpha\beta}. \quad (\text{A}\cdot 15)$$

Then the NZH reduction formula is summarized as

$$\begin{aligned} & \sqrt{Z} \left[T(\mathcal{O}) B_{\text{in}}^\dagger(\mathbf{p}, s) - (-)^{|\mathcal{O}|} B_{\text{out}}^\dagger(\mathbf{p}, s) T(\mathcal{O}) \right] \\ &= \int d^4x e^{-ipx} T\{\mathcal{O} \bar{N}(x)\} [-iS^{-1}(p)u(\mathbf{p}, s)], \end{aligned} \quad (\text{A}\cdot 16)$$

$$\begin{aligned} & \sqrt{Z} \left[B_{\text{out}}(\mathbf{p}, s) T(\mathcal{O}) - (-)^{|\mathcal{O}|} T(\mathcal{O}) B_{\text{in}}(\mathbf{p}, s) \right] \\ &= \int d^4x e^{ipx} [-i\bar{u}(\mathbf{p}, s)S^{-1}(p)] T\{N(x)\mathcal{O}\}. \end{aligned} \quad (\text{A}\cdot 17)$$

Here \mathcal{O} is an arbitrary product of operators with the number of fermionic operators denoted by $|\mathcal{O}|$, and $S^{-1}(p) = (\cancel{p} - m + i\delta)$ is the inverse of the free nucleon propagator. The asymptotic baryon and anti-baryon operators, $B_{\text{as}}(\mathbf{p}, s)$ and $D_{\text{as}}(\mathbf{p}, s)$ (as = in, out) are defined by the Fourier decomposition of $N_{\text{as}}(x)$,

$$N_{\text{as}}(x) = \sum_s \int \frac{d^3p}{(2\pi)^3 2\varepsilon_p} \left[e^{-ipx} B_{\text{as}}(\mathbf{p}, s) u(\mathbf{p}, s) + e^{ipx} D_{\text{as}}^\dagger(\mathbf{p}, s) v(\mathbf{p}, s) \right], \quad (\text{A}\cdot 18)$$

where the flavor and spinor indices are suppressed. The operator B_{as} thus defined satisfies the covariant commutation relation, $\{B_{\text{as}}(\mathbf{p}, s), B_{\text{as}}^\dagger(\mathbf{p}', s')\} = 2\varepsilon_p(2\pi)^3\delta_{ss'}\delta^3(\mathbf{p}-\mathbf{p}')$, and asymptotic states are defined by $|B(\mathbf{p}, s)\rangle_{\text{as}} = B_{\text{as}}^\dagger(\mathbf{p}, s)|0\rangle$.

By using the NZH reduction formula, we can evaluate our BS amplitude Eq. (A.12) as

$$\begin{aligned} \Psi_{12}(x_1, x_2) = \\ Z^{-1} \int \prod_{i=1}^2 \left\{ \frac{d^4 q_i}{(2\pi)^4} e^{-iq_i x_i} \right\} G_{12;34}(q_1, q_2; q_3, q_4) [-iS^{-1}(q_3)u(3)]_3 [-iS^{-1}(q_4)u(4)]_4, \end{aligned} \quad (\text{A.19})$$

where the four-point Green's function is defined by

$$G_{12;34}(q_1, q_2; q_3, q_4) = \int \prod_{i=1}^4 \{d^4 x_i e^{iq_i x_i}\} \langle 0 | T \{ n_2(x_2) p_1(x_1) \bar{p}_3(x_3) \bar{n}_4(x_4) \} | 0 \rangle. \quad (\text{A.20})$$

Here, to simplify the notation, we abbreviate the Lorentz indices by the lower-case suffixes $(1, \dots, 4)$ with the repeated suffixes being contracted and the state labels are abbreviated as the numbers in the parenthesis, e.g. $u_\alpha(\mathbf{q}, s) \rightarrow u_3(3)$ and $u_\beta(\mathbf{q}', s') \rightarrow u_4(4)$. The four-point function can be decomposed into the free part and the connected part as $G_{12;34} = Z^2(G_{12;34}^{(0)} + G_{12;34}^{(c)})$. The free part reads

$$G_{12;34}^{(0)} = (2\pi)^8 \delta^4(q_1 - q_3) \delta^4(q_2 - q_4) [iS(q_3)]_{13} [iS(q_4)]_{24}, \quad (\text{A.21})$$

whereas the connected part is rewritten with the proper vertex Γ as

$$\begin{aligned} G_{12;34}^{(c)}(q_1, q_2; q_3, q_4) \\ = (2\pi)^4 \delta^4(K - Q) [iS(q_1)]_{11'} [iS(q_2)]_{22'} (-i)\Gamma_{1'2';3'4'}(k; q|Q) [iS(q_3)]_{3'3} [iS(q_4)]_{4'4}. \end{aligned} \quad (\text{A.22})$$

Here we have introduced relative and center-of-mass (c.m.) 4-momenta by

$$K = q_1 + q_2, \quad k = (q_1 - q_2)/2, \quad Q = q_3 + q_4, \quad q = (q_3 - q_4)/2. \quad (\text{A.23})$$

Then, the K -integration in Eq. (A.19) can be carried out to obtain

$$\Psi_{12}(x_1, x_2) = \left[\psi_{12}^{(0)}(r) + \psi_{12}^{(c)}(r) \right] e^{-iQR}, \quad (\text{A.24})$$

$$\psi_{12}^{(0)}(r) = Z u_1(3) u_2(4) e^{-iqr}, \quad (\text{A.25})$$

$$\psi_{12}^{(c)}(r) = iZ \int \frac{d^4 k}{(2\pi)^4} e^{-ikr} [S(q_1)]_{11'} [S(q_2)]_{22'} \Gamma_{1'2';34}(k; q|Q) u_3(3) u_4(4), \quad (\text{A.26})$$

where $r = x_1 - x_2$ and $R = (x_1 + x_2)/2$ are relative and c.m. 4-dimensional coordinates, respectively. Covariant Nambu-Bethe-Salpeter type differential equation can

be obtained by multiplying $S^{-1}(i\vec{\partial}_1)S^{-1}(i\vec{\partial}_2)$ to Eqs. (A·24)–(A·26) from the left:

$$\begin{aligned} & [S^{-1}(i\vec{\partial}_x)]_{\alpha\alpha'} [S^{-1}(i\vec{\partial}_y)]_{\beta\beta'} \Psi_{\alpha'\beta'}(x, y) \\ &= iZ \int \frac{d^4k}{(2\pi)^4} e^{-ikr} e^{-iQR} \Gamma_{\alpha\beta;\gamma\delta}(k; q|Q) u_\gamma(\mathbf{q}, s) u_\delta(\mathbf{q}', s'). \end{aligned} \quad (\text{A}\cdot 27)$$

In our applications of the NN scattering at low energies, it is useful to consider the equal-time BS amplitude (which we call the BS wave function in the text) and associated Lippmann-Schwinger type integral equation or the Schrödinger type differential equation. For this purpose, we first carry out the integration over k^0 in Eq. (A·26) using the explicit form of the free propagator:

$$S(p) = \left(\frac{1}{\not{p} - m + i\delta} \right)_{\alpha\beta} = \frac{1}{2\varepsilon_p} \left[\frac{\sum_s u_\alpha(\mathbf{p}, s) \bar{u}_\beta(\mathbf{p}, s)}{p^0 - \varepsilon_p + i\delta} + \frac{\sum_s v_\alpha(-\mathbf{p}, s) \bar{v}_\beta(-\mathbf{p}, s)}{p^0 + \varepsilon_p - i\delta} \right]. \quad (\text{A}\cdot 28)$$

Since we are interested in the asymptotic form of the wave function at $|\mathbf{r}| \rightarrow \infty$ below pion production threshold, we can pick up only the nucleon pole from $S(p)$ in the k^0 -integral of Eq. (A·26) without loss of generality. Possible poles from Γ associated with the resonance production and with the deuteron bound state, as well as anti-nucleon poles in $S(p)$ in Eq. (A·28), modify only the short-distant part of the wave function. This does not at all imply that those contributions are not important. They do affect the actual values of the phase shifts and mixing parameters and are fully taken into account in the definition of our potential, Eqs. (3·3) and (3·4).

Using the residue theorem and taking the equal-time limit ($x_0 = y_0 \equiv t$) in the rest frame of the two-particles ($\mathbf{Q} = 0$), we end up with the Lippmann-Schwinger type equation;

$$\Psi_{\alpha\beta}(\mathbf{r}, t) = \psi_{\alpha\beta}(\mathbf{r}; \mathbf{q}, s, s') e^{-2i\varepsilon_q t}, \quad (\text{A}\cdot 29)$$

$$\psi_{\alpha\beta}^{(0)}(\mathbf{r}; \mathbf{q}, s, s') = Z u_\alpha(\mathbf{q}, s) u_\beta(-\mathbf{q}, s') e^{i\mathbf{q}\cdot\mathbf{r}}, \quad (\text{A}\cdot 30)$$

$$\begin{aligned} \psi_{\alpha\beta}(\mathbf{r}; \mathbf{q}, s, s') = & \psi_{\alpha\beta}^{(0)}(\mathbf{r}; \mathbf{q}, s, s') \\ & + \sum_{\tilde{s}, \tilde{s}'} \int \frac{d^3k}{(2\pi)^3} \psi_{\alpha\beta}^{(0)}(\mathbf{r}; \mathbf{k}, \tilde{s}, \tilde{s}') \frac{\varepsilon_q + \varepsilon_k}{8\varepsilon_k^2} \frac{\mathcal{T}_{\tilde{s}\tilde{s}'; ss'}(\mathbf{k}; \mathbf{q})}{\mathbf{k}^2 - \mathbf{q}^2 - i\delta} + \mathcal{I}(\mathbf{r}). \end{aligned} \quad (\text{A}\cdot 31)$$

Here $\mathcal{I}(\mathbf{r})$ originates from the contributions other than the nucleon pole and is an exponentially localized function in \mathbf{r} below inelastic threshold.⁴⁷⁾ In Eq. (A·31), we have defined the half off-shell T -matrix,

$$i\mathcal{T}_{12;34}(\mathbf{k}; \mathbf{q}) = \bar{u}_1(1) \bar{u}_2(2) (-i) \Gamma_{12;34}(k; q|Q) u_3(3) u_4(4), \quad (\text{A}\cdot 32)$$

where the outgoing energy $2\varepsilon_k = 2\sqrt{\mathbf{k}^2 + m^2}$ is not necessary equal to the incoming energy $2\varepsilon_q = 2\sqrt{\mathbf{q}^2 + m^2}$. The Schrödinger type differential equation is obtained from Eq. (A·31) by multiplying $\mathbf{q}^2 + \nabla^2$,

$$(\mathbf{q}^2 + \nabla^2) \psi_{\alpha\beta}(\mathbf{r}; \mathbf{q}, s, s') = - \sum_{\tilde{s}, \tilde{s}'} \int \frac{d^3k}{(2\pi)^3} \psi_{\alpha\beta}^{(0)}(\mathbf{r}; \mathbf{k}, \tilde{s}, \tilde{s}') \frac{\varepsilon_q + \varepsilon_k}{8\varepsilon_k^2} \mathcal{T}_{\tilde{s}\tilde{s}'; ss'}(\mathbf{k}; \mathbf{q}) + \mathcal{K}(\mathbf{r}), \quad (\text{A}\cdot 33)$$

with $\mathcal{K}(\mathbf{r}) = (\mathbf{q}^2 + \nabla^2)\mathcal{I}(\mathbf{r})$. Since the plain wave part of $\psi_{\alpha\beta}(\mathbf{r}; \mathbf{q}, s, s')$ is projected out by the operator $(\mathbf{q}^2 + \nabla^2)$, the right-hand side of Eq. (A·33) is exponentially localized in \mathbf{r} and vanishes for $r > R$.

A.3. Asymptotic BS wave function and the phase shift

Let us further consider the asymptotic behaviour of $\psi_{\alpha\beta}(\mathbf{r}; \mathbf{q}, s, s')$ at large r to relate it to the scattering parameters (phase shifts and mixing angles) defined in §A.1. The derivation of this subsection has been essentially given by Ishizuka in Ref. 38).

To perform the \mathbf{k} integration in Eq. (A·33), we introduce the following helicity decomposition of the half-off shell T -matrix,

$$\mathcal{T}_{s_1 s_2; s_3 s_4}(\mathbf{k}, \mathbf{q}) = 4\pi \sum_{J, M} \frac{2J+1}{4\pi} \langle s_1, s_2 | T^J(k; q) | s_3, s_4 \rangle (D^J)_{sM}^\dagger(\Omega_k) D_{Ms'}^J(\Omega_q), \quad (\text{A} \cdot 34)$$

$$u_\alpha(\mathbf{k}, s_1) u_\beta(-\mathbf{k}, s_2) e^{i\mathbf{k} \cdot \mathbf{r}} = \sum_{JM} D_{Ms}^J(\Omega_k) U_{\alpha a}(\nabla) U_{\beta b}(-\nabla) \phi_{JM s_1 s_2; ab}^{[j]}(\mathbf{r}, k), \quad (\text{A} \cdot 35)$$

where $s = s_1 - s_2$, $s' = s_3 - s_4$, $k = |\mathbf{k}|$ and $q = |\mathbf{q}|$. The reduced wave function $\phi^{[j]}$ in the 2×2 spinor space labeled by the indices a, b is defined as

$$\begin{aligned} \phi_{JM \lambda_1 \lambda_2}^{[j]}(\mathbf{r}, k) &= \sum_{\ell, s} \phi_{JM \ell s}^{[j]}(\mathbf{r}, k) \langle JM \ell s | JM \lambda_1 \lambda_2 \rangle, \\ \phi_{JM \ell s}^{[j]}(\mathbf{r}, k) &= j_\ell(kr) Y_{JM}^{\ell s}(\Omega_r), \quad Y_{JM}^{\ell s}(\Omega_r) = \sum_{\ell_z s_z} Y_{\ell \ell_z}(\Omega_r) \chi(s, s_z) \langle \ell s \ell_z s_z | JM \rangle. \end{aligned} \quad (\text{A} \cdot 36)$$

Note that $U_{\alpha a}(\nabla)$ and $U_{\beta b}(-\nabla)$ in Eq. (A·35) are the 4×2 matrices acting on the 2×2 matrix $\phi_{ab}^{[j]}$ so that the Dirac structure $u_\alpha(\mathbf{k}, s_1) u_\beta(-\mathbf{k}, s_2)$ is correctly reproduced: Explicitly, $U(\nabla) = \sqrt{(\varepsilon_k + m_N)}(I_{2 \times 2} - i\boldsymbol{\sigma} \cdot \nabla / (\varepsilon_k + m_N))$. Alternatively, one may use the Lorentz transformation, $u(\mathbf{p}, s) = \Lambda(\mathbf{p})u(\mathbf{0}, s)$ to define the reduced wave function.⁴⁸⁾

Note that $\langle JM \ell s | JM \lambda_1 \lambda_2 \rangle$ in Eq. (A·36) is a transformation function between the helicity basis and the orbital-spin basis at fixed J, M .⁴⁶⁾ Also, $\chi_{ab}(s, s_z)$ in Eq. (A·37) is a 2×2 matrix in the spinor space with total spin $s = 1$ or 0 and its z -component s_z , and $j_\ell(x)$ is a spherical Bessel function. Using Eq. (A·8), Eq. (A·31) for large r becomes

$$\begin{aligned} \psi(\mathbf{r}; \mathbf{q}, s, s') &= Z \sum_{JM} D_{M\lambda}^J(\Omega_q) U(\nabla) U(-\nabla) \psi_{JM ss'}(\mathbf{r}; q), \quad \lambda = s - s', \quad (\text{A} \cdot 38) \\ \psi_{JM ss'}(\mathbf{r}; q) &\xrightarrow{r > R} \phi_{JM ss'}^{[j]}(\mathbf{r}, q) + \sum_{\tilde{s}, \tilde{s}'} \int_0^\infty \frac{k^2 dk}{2\pi^2} \phi_{JM \tilde{s} \tilde{s}'}^{[j]}(\mathbf{r}, k) \frac{\varepsilon_q + \varepsilon_k}{8\varepsilon_k^2} \frac{\langle \tilde{s} \tilde{s} | T^J(k; q) | ss' \rangle}{k^2 - q^2 - i\delta}. \end{aligned} \quad (\text{A} \cdot 39)$$

To evaluate the integral in Eq. (A·39), we use the following formula^{37),38)} valid for $r > R$ in which $\int_0^\infty f(k)k^{-\ell}j_0(kr)k^2dk = 0$ is satisfied:*)

$$\int_0^\infty \frac{k^2 dk}{2\pi^2} \frac{j_\ell(kr)f(k)}{k^2 - q^2 - i\delta} = i \frac{q}{4\pi} h_\ell^{(+)}(qr)f(q). \quad (\text{A} \cdot 40)$$

Here $h_\ell^{(\pm)}(x) (\equiv j_\ell(x) \pm i n_\ell(x))$ is the spherical Hankel function with $j_0(x) = (\sin x)/x$ and $n_0(x) = -(\cos x)/x$, so that $h_\ell^{(+)}(qr)$ represents the spherical outgoing-wave.

Then, we obtain

$$\begin{aligned} \psi_{JMss'}(\mathbf{r}; q) &\xrightarrow{r>R} \phi_{JMss'}^{[j]}(\mathbf{r}, q) + i \sum_{\tilde{s}, \tilde{s}'} \frac{q}{16\pi\epsilon_q} \phi_{JM\tilde{s}\tilde{s}'}^{[h^{(+)}]}(\mathbf{r}, q) \langle \tilde{s}\tilde{s} | T^J(q; q) | ss' \rangle \\ &= \sum_{\tilde{s}, \tilde{s}'} \left[\phi_{JM\tilde{s}\tilde{s}'}^{[j]}(\mathbf{r}, q) A_{\tilde{s}\tilde{s}'; ss'}^J(q) - \phi_{JM\tilde{s}\tilde{s}'}^{[n]}(\mathbf{r}, q) B_{\tilde{s}\tilde{s}'; ss'}^J(q) \right], \quad (\text{A} \cdot 41) \end{aligned}$$

$$A^J(q) = 1 + i \frac{q}{16\pi\epsilon_q} T^J(q; q), \quad B^J(q) = \frac{q}{16\pi\epsilon_q} T^J(q; q), \quad (\text{A} \cdot 42)$$

where $\phi_{JM\tilde{s}\tilde{s}'}^{[n, h^{(+)}]}(\mathbf{r}, q)$ is obtained from $\phi_{JM\tilde{s}\tilde{s}'}^{[j]}(\mathbf{r}, q)$ by the replacement $j_\ell(kr) \rightarrow n_\ell(qr), h_\ell^{(+)}(qr)$.

Using the explicit form of the T -matrix given in (A·11), we finally obtain

$$X_{\ell=J, s}^J = \hat{X}_{Js}, \quad X_{\ell=J\mp 1, s=1}^J = O(q) \begin{pmatrix} \hat{X}_{J-1, 1} & 0 \\ 0 & \hat{X}_{J+1, 1} \end{pmatrix} O^{-1}(q), \quad (\text{A} \cdot 43)$$

with X being either A or B , and

$$\hat{A}_{\ell s}(q) = e^{i\delta_{\ell s}(q)} \cos \delta_{\ell s}(q), \quad \hat{B}_{\ell s}(q) = e^{i\delta_{\ell s}(q)} \sin \delta_{\ell s}(q), \quad (\text{A} \cdot 44)$$

$$\frac{\hat{A}_{\ell s}(q)}{\hat{B}_{\ell s}(q)} = \frac{1}{\tan \delta_{\ell s}(q)}. \quad (\text{A} \cdot 45)$$

We now have shown that the BS wave function in QCD has an asymptotic form of the scattering wave of the quantum mechanics at large r . To derive this we have only use the unitary of the S -matrix below the inelastic threshold, and have identified the phase of the S -matrix as the scattering phase shift of the asymptotic BS wave function. This observation leads to the important conclusion that the potential defined through the BS wave function, by construction, gives the correct scattering phase shift at asymptotically large r .

Appendix B

—— Okubo-Marshak Decomposition ——

In this appendix, we derive the general form of the NN potential in the space of two-component spinors, following the argument by Okubo and Marshak.²⁵⁾ The

*) Since the nucleons are non-interacting in the asymptotic region, the right hand side of Eq. (A·33) is exponentially small for $r > R$. This gives a little weaker condition that $\int_0^\infty f(k)j_\ell(kr)k^2dk = 0$, which, together with some properties of the T -matrix, leads to the stronger condition used here.

general form of the 2-body potential with derivatives reads

$$V(\mathbf{r}_1, \mathbf{r}_2, \mathbf{v}_1, \mathbf{v}_2, \boldsymbol{\sigma}_1, \boldsymbol{\sigma}_2, \boldsymbol{\tau}_1, \boldsymbol{\tau}_2, t), \quad (\text{B}\cdot 1)$$

where $\mathbf{v}_{1,2} = \mathbf{p}_{1,2}/m_N$.

There are several conditions to be satisfied by V .

1. Probability conservation: This leads to the hermiticity of the potential: $V^\dagger = V$.
2. Energy-momentum conservation: The energy conservation demands that the potential does not depend on time explicitly. The momentum conservation leads the translational invariance of the potential. Thus we have

$$V = V(\mathbf{r}, \mathbf{v}_1, \mathbf{v}_2, \boldsymbol{\sigma}_1, \boldsymbol{\sigma}_2, \boldsymbol{\tau}_1, \boldsymbol{\tau}_2), \quad (\text{B}\cdot 2)$$

where $\mathbf{r} = \mathbf{r}_1 - \mathbf{r}_2$.

3. Galilei invariance: The potential is assumed to be independent of the center of mass momentum of the two-body system, which leads to

$$V = V(\mathbf{r}, \mathbf{v}, \boldsymbol{\sigma}_1, \boldsymbol{\sigma}_2, \boldsymbol{\tau}_1, \boldsymbol{\tau}_2), \quad (\text{B}\cdot 3)$$

where $\mathbf{v} = \mathbf{p}/\mu = (\mathbf{p}_1 - \mathbf{p}_2)/(2\mu) = \mathbf{v}_1 - \mathbf{v}_2$.

4. Conservation of total-angular momentum: The total angular momentum is defined as $\mathbf{J} = \mathbf{S} + \mathbf{L}$ with

$$\mathbf{S} = \frac{1}{2}(\boldsymbol{\sigma}_1 + \boldsymbol{\sigma}_2), \quad \mathbf{L} = \mathbf{r} \times \mathbf{p}. \quad (\text{B}\cdot 4)$$

The potential is a scalar under the spatial rotation. Then, V is the scalar functions of $\mathbf{r}, \mathbf{v}, \boldsymbol{\sigma}_1$ and $\boldsymbol{\sigma}_2$.

5. Parity invariance: The strong interaction conserves parity. Thus V is invariant under reflection, $\mathbf{r} \rightarrow -\mathbf{r}$ and $\mathbf{v} \rightarrow -\mathbf{v}$,

$$V(\mathbf{r}, \mathbf{v}, \boldsymbol{\sigma}_1, \boldsymbol{\sigma}_2, \boldsymbol{\tau}_1, \boldsymbol{\tau}_2) = V(-\mathbf{r}, -\mathbf{v}, \boldsymbol{\sigma}_1, \boldsymbol{\sigma}_2, \boldsymbol{\tau}_1, \boldsymbol{\tau}_2). \quad (\text{B}\cdot 5)$$

6. Time-reversal invariance: The strong interaction preserves time-reflection symmetry under $\mathbf{r} \rightarrow \mathbf{r}, \mathbf{v} \rightarrow -\mathbf{v}, \boldsymbol{\sigma}_i \rightarrow -\boldsymbol{\sigma}_i$, which leads to

$$V(\mathbf{r}, \mathbf{v}, \boldsymbol{\sigma}_1, \boldsymbol{\sigma}_2, \boldsymbol{\tau}_1, \boldsymbol{\tau}_2) = V(\mathbf{r}, -\mathbf{v}, -\boldsymbol{\sigma}_1, -\boldsymbol{\sigma}_2, \boldsymbol{\tau}_1, \boldsymbol{\tau}_2). \quad (\text{B}\cdot 6)$$

7. Fermi statistics: The potential is invariant under the permutation of the particle coordinates,

$$V(\mathbf{r}, \mathbf{v}, \boldsymbol{\sigma}_1, \boldsymbol{\sigma}_2, \boldsymbol{\tau}_1, \boldsymbol{\tau}_2) = V(-\mathbf{r}, -\mathbf{v}, \boldsymbol{\sigma}_2, \boldsymbol{\sigma}_1, \boldsymbol{\tau}_2, \boldsymbol{\tau}_1) = V(\mathbf{r}, \mathbf{v}, \boldsymbol{\sigma}_2, \boldsymbol{\sigma}_1, \boldsymbol{\tau}_2, \boldsymbol{\tau}_1), \quad (\text{B}\cdot 7)$$

where parity invariance was used in the second equality.

8. Isospin invariance: The potential is invariant under the rotation in isospin space, which leads to two independent potentials $V^{I=0,1}$,

$$V = V^0(\mathbf{r}, \mathbf{v}, \boldsymbol{\sigma}_1, \boldsymbol{\sigma}_2)P_0^\tau + V^1(\mathbf{r}, \mathbf{v}, \boldsymbol{\sigma}_1, \boldsymbol{\sigma}_2)P_1^\tau. \quad (\text{B}\cdot 8)$$

9. Furthermore, V has only the terms $\sigma_1^n \sigma_2^m$ with $(n, m) = (0, 0), (1, 0), (0, 1), (1, 1)$.

The other higher order terms can be always reduced to the above form because of the property of the Pauli matrices: $\sigma_i \sigma_j = \delta_{ij} + i\varepsilon_{ijk} \sigma_k$.

Then, the terms which have Pauli matrices and satisfy the above constraints are restricted only to the following combinations:

$$\boldsymbol{\sigma}_1 \cdot \boldsymbol{\sigma}_2, \quad (\boldsymbol{\sigma}_1 + \boldsymbol{\sigma}_2) \cdot \mathbf{L}, \quad (\boldsymbol{\sigma}_1 \cdot \mathbf{r})(\boldsymbol{\sigma}_2 \cdot \mathbf{r}), \quad (\text{B}\cdot\text{9})$$

$$(\boldsymbol{\sigma}_1 \cdot \mathbf{v})(\boldsymbol{\sigma}_2 \cdot \mathbf{v}), \quad (\boldsymbol{\sigma}_1 \cdot \mathbf{L})(\boldsymbol{\sigma}_2 \cdot \mathbf{L}). \quad (\text{B}\cdot\text{10})$$

It is sometimes convenient to reorganize the above 5 terms into the following hermitian operators:

$$\begin{aligned} \boldsymbol{\sigma}_1 \cdot \boldsymbol{\sigma}_2, \quad S_{12} &\equiv 3(\boldsymbol{\sigma}_1 \cdot \hat{\mathbf{r}})(\boldsymbol{\sigma}_2 \cdot \hat{\mathbf{r}}) - \boldsymbol{\sigma}_1 \cdot \boldsymbol{\sigma}_2, \\ \mathbf{L} \cdot \mathbf{S}, \\ P_{12} &\equiv (\boldsymbol{\sigma}_1 \cdot \mathbf{v})(\boldsymbol{\sigma}_2 \cdot \mathbf{v}), \quad W_{12} \equiv Q_{12} - \frac{1}{3}(\boldsymbol{\sigma}_1 \cdot \boldsymbol{\sigma}_2)\mathbf{L}^2, \end{aligned} \quad (\text{B}\cdot\text{11})$$

where

$$Q_{12} \equiv \frac{1}{2} [(\boldsymbol{\sigma}_1 \cdot \mathbf{L})(\boldsymbol{\sigma}_2 \cdot \mathbf{L}) + (\boldsymbol{\sigma}_2 \cdot \mathbf{L})(\boldsymbol{\sigma}_1 \cdot \mathbf{L})]. \quad (\text{B}\cdot\text{12})$$

In Q_{12} the spins need to be symmetrized to make it hermitian since L_i and L_j do not commute with each other. Note that the term such as $(\mathbf{S} \cdot \mathbf{L})^2$ can be decomposed into Q_{12} , $\mathbf{S} \cdot \mathbf{L}$ and spin-independent \mathbf{L}^2 term.

We decompose V^0 and V^1 in terms of the above operators with coefficients V_A^I ($I = (0, 1)$, $A = (0, \sigma, T, LS, P, W)$) which are the scalar function made of \mathbf{r} and \mathbf{v} satisfying the general constraints;

$$V_A^I = V_A^I(\mathbf{r}^2, \mathbf{v}^2, \mathbf{L}^2). \quad (\text{B}\cdot\text{13})$$

Note that the scalar $(\mathbf{r} \cdot \mathbf{p})^2$ can be written by $\mathbf{r}^2 \mathbf{p}^2$ and \mathbf{L}^2 .

Combining all, we arrive at the general decomposition given in §4.

Appendix C

—— Matrix Element of the Potential ——

In this appendix, we consider the partial wave decomposition of the general form of the NN potential. At given J , there are 2 distinct states, the spin-singlet ($s = 0$) state and the spin-triplet ($s = 1$) state. We now consider how the five operators in Eq. (B·11) act on these states.

The singlet state is denoted as 1J_J , since it has $s = 0$ and $J = \ell$. The fact that $I + \ell + s$ must be odd to satisfy fermion anti-symmetry gives $I = 0$ for odd J and $I = 1$ for even J . The eigenstate with $J_z = M$ can be easily obtained as

$$|^1J_J, M\rangle = |M, 0\rangle_{J,0}, \quad (\text{C}\cdot\text{1})$$

where we use the short-handed notation, $|J_z, s_z\rangle_{J,s} = |J, J_z\rangle \otimes |s, s_z\rangle$.

The spin-triplet state is classified into 3 types: 3J_J , ${}^3(J \pm 1)_J$. For the first one, $I = 0$ (even J) or $I = 1$ (odd J), and vice versa for other two types. By the Wigner-Eckart theorem, the matrix elements of the five operators do not depend on J_z . Therefore it is enough to know eigenstates with $J_z = J$ only. Explicitly we have

$$|{}^3J_J, J\rangle = \frac{1}{\sqrt{J+1}} \left\{ |J-1, 1\rangle_{J,1} - \sqrt{J} |J, 0\rangle_{J,1} \right\}, \quad (\text{C}\cdot 2)$$

$$|{}^3(J-1)_J, J\rangle = |J-1, 1\rangle_{J-1,1}, \quad (\text{C}\cdot 3)$$

$$|{}^3(J+1)_J, J\rangle = \frac{1}{\sqrt{(J+1)(2J+3)}} \left\{ |J-1, 1\rangle_{J+1,1} + \sqrt{2J+1} \left[\sqrt{(J+1)} |J+1, -1\rangle_{J+1,1} - |J, 0\rangle_{J+1,1} \right] \right\}. \quad (\text{C}\cdot 4)$$

Using these eigenstates, it is easy to see

$$\boldsymbol{\sigma}_1 \cdot \boldsymbol{\sigma}_2 = 2s(s+1) - 3 = -3, \quad 1, \quad 1, \quad 1, \quad (\text{C}\cdot 5)$$

$$\mathbf{L} \cdot \mathbf{S} = \frac{J(J+1) - \ell(\ell+1) - s(s+1)}{2} = 0, \quad -1, \quad J-1, \quad -(J+2), \quad (\text{C}\cdot 6)$$

$$W_{12} = 0, \quad -\frac{(2J-1)(2J+3)}{3}, \quad \frac{(J-1)(2J-3)}{3}, \quad \frac{(J+2)(2J+5)}{3}, \quad (\text{C}\cdot 7)$$

for 1J_J , 3J_J , ${}^3(J-1)_J$ and ${}^3(J+1)_J$, respectively.

For S_{12} and P_{12} results are more complicated due to the mixing between ${}^3(J-1)_J$ and ${}^3(J+1)_J$. After a little algebra we obtain

$$S_{12} = 0, \quad 2, \quad \begin{pmatrix} -\frac{2(J-1)}{2J+1}, & \frac{6\sqrt{J(J+1)}}{2J+1} \\ \frac{6\sqrt{J(J+1)}}{2J+1}, & -\frac{2(J+2)}{2J+1} \end{pmatrix}, \quad (\text{C}\cdot 8)$$

$$\mu^2 P_{12} = 0, \quad 2p_J^2, \quad \begin{pmatrix} -\frac{2(J-1)}{2J+1} p_{J-1}^2, & \frac{6\sqrt{J(J+1)}}{2J+1} p_+^2 \\ \frac{6\sqrt{J(J+1)}}{2J+1} p_-^2, & -\frac{2(J+2)}{2J+1} p_{J+1}^2 \end{pmatrix}, \quad (\text{C}\cdot 9)$$

where

$$p_\ell^2 = p_r^2 - i\frac{2}{r}p_r + \frac{\ell(\ell+1)}{r^2} \equiv \mu^2 v_\ell^2, \quad (\text{C}\cdot 10)$$

$$p_+^2 = \left(p_r - i\frac{J+1}{r} \right) \left(p_r - i\frac{J+2}{r} \right) \equiv \mu^2 v_+^2, \quad (\text{C}\cdot 11)$$

$$p_-^2 = \left(p_r + i\frac{J}{r} \right) \left(p_r + i\frac{J-1}{r} \right) \equiv \mu^2 v_-^2, \quad (\text{C}\cdot 12)$$

with $\ell = J \pm 1$ and $ip_r = \partial/(\partial r)$.

Using these results, we obtain the potential for each channel: We have

$$V[{}^1J_J] = V_0^I(r^2, v_J^2, \hat{J}^2) + V_\sigma^I(r^2, v_J^2, \hat{J}^2), \quad \hat{J}^2 = J(J+1) \quad (\text{C}\cdot 13)$$

for the 1J_J state, and

$$V[{}^3J_J] = V_0^{\bar{I}}(r^2, v_J^2, \hat{J}^2) - 3V_\sigma^{\bar{I}}(r^2, v_J^2, \hat{J}^2) - V_{LS}^{\bar{I}}(r^2, v_J^2, \hat{J}^2) + 2V_T^{\bar{I}}(r^2, v_J^2, \hat{J}^2) \\ - \frac{(2J-1)(2J+3)}{3} V_W^{\bar{I}}(r^2, v_J^2, \hat{J}^2) + \{V_P^{\bar{I}}(r^2, v_J^2, \hat{J}^2), v_J^2\} \quad (\text{C}\cdot 14)$$

for the 3J_J state, where $\bar{I} = 1 - I$.

For ${}^3(J \mp 1)_J$, the result is more involved:

$$V[{}^3(J \mp 1)_J] = \begin{pmatrix} V_{--} & V_{-+} \\ V_{+-} & V_{++} \end{pmatrix}, \quad (\text{C}\cdot 15)$$

where

$$V_{--} = V_0^I(r^2, v_{J_-}^2, \hat{J}_-^2) - 3V_\sigma^I(r^2, v_{J_-}^2, \hat{J}_-^2) + (J-1)V_{LS}^I(r^2, v_{J_-}^2, \hat{J}_-^2) \\ - \frac{(J-1)(2J-3)}{3} V_W^I(r^2, v_{J_-}^2, \hat{J}_-^2) \\ - \frac{J-1}{2J+1} \left[2V_T^I(r^2, v_{J_-}^2, \hat{J}_-^2) + \{V_P^I(r^2, v_{J_-}^2, \hat{J}_-^2), v_{J_-}^2\} \right], \quad (\text{C}\cdot 16)$$

$$V_{++} = V_0^I(r^2, v_{J_+}^2, \hat{J}_+^2) - 3V_\sigma^I(r^2, v_{J_+}^2, \hat{J}_+^2) - (J+2)V_{LS}^I(r^2, v_{J_+}^2, \hat{J}_+^2) \\ + \frac{(J+2)(2J+5)}{3} V_W^I(r^2, v_{J_+}^2, \hat{J}_+^2) \\ - \frac{J+2}{2J+1} \left[2V_T^I(r^2, v_{J_+}^2, \hat{J}_+^2) + \{V_P^I(r^2, v_{J_+}^2, \hat{J}_+^2), v_{J_+}^2\} \right], \quad (\text{C}\cdot 17)$$

$$V_{-+} = \frac{3\sqrt{J(J+1)}}{2(2J+1)} \left[2V_T^I(r^2, v_{J_+}^2, \hat{J}_+^2) + 2V_T^I(r^2, v_{J_-}^2, \hat{J}_-^2) \right. \\ \left. + v_+^2 V_P^I(r^2, v_{J_-}^2, \hat{J}_-^2) + v_+^2 V_P^I(r^2, v_{J_+}^2, \hat{J}_+^2) v_+^2 \right], \quad (\text{C}\cdot 18)$$

$$V_{+-} = \frac{3\sqrt{J(J+1)}}{2(2J+1)} \left[2V_T^I(r^2, v_{J_+}^2, \hat{J}_+^2) + 2V_T^I(r^2, v_{J_-}^2, \hat{J}_-^2) \right. \\ \left. + v_-^2 V_P^I(r^2, v_{J_-}^2, \hat{J}_-^2) + v_-^2 V_P^I(r^2, v_{J_+}^2, \hat{J}_+^2) \right], \quad (\text{C}\cdot 19)$$

where $J_\pm = J \pm 1$ and $\hat{J}_\pm^2 = J_\pm(J_\pm + 1)$. Note that $V_{+-} = (V_{-+})^\dagger$ with r^2 from the integration measure.

Appendix D

—— Heat-Kernel Representation of the Green's Function ——

We define the heat kernel $\mathcal{K}(t, \mathbf{x})$ through the initial value problem as

$$\frac{\partial}{\partial t} \mathcal{K}(t, \mathbf{x}) = \nabla^2 \mathcal{K}(t, \mathbf{x}), \quad \lim_{t \rightarrow 0^+} \mathcal{K}(t, \mathbf{x}) = \delta_{\text{lat}}(\mathbf{x}), \quad (\text{D}\cdot 1)$$

where $\delta_{\text{lat}}(\mathbf{x}) \equiv \frac{1}{L^3} \sum_{\mathbf{n} \in \mathbf{Z}^3} e^{2\pi i \mathbf{n} \cdot \mathbf{x}/L}$ denotes the delta function in a periodic box of spatial extension L . $\mathcal{K}(t, \mathbf{x})$ is explicitly expressed as

$$\mathcal{K}(t, \mathbf{x}) = e^{t\nabla^2} \delta_{\text{lat}}(\mathbf{x}) = \frac{1}{L^3} \sum_{\mathbf{n} \in \mathbf{Z}^3} \exp(-t(2\pi/L)^2 \mathbf{n}^2 + 2\pi i \mathbf{n} \cdot \mathbf{x}/L). \quad (\text{D}\cdot 2)$$

For convenience, we define a modified heat kernel $\tilde{\mathcal{K}}(t, \mathbf{x}; k^2)$ as

$$\tilde{\mathcal{K}}(t, \mathbf{x}; k^2) \equiv e^{tk^2} \mathcal{K}(t, \mathbf{x}), \quad (\text{D}\cdot 3)$$

which is the solution to the equation that

$$\frac{\partial}{\partial t} \tilde{\mathcal{K}}(t, \mathbf{x}; k^2) = (\nabla^2 + k^2) \tilde{\mathcal{K}}(t, \mathbf{x}; k^2), \quad \lim_{t \rightarrow 0^+} \tilde{\mathcal{K}}(t, \mathbf{x}; k^2) = \delta_{\text{lat}}(\mathbf{x}). \quad (\text{D}\cdot 4)$$

An integration from 0 to s leads us to

$$\tilde{\mathcal{K}}(s, \mathbf{x}; k^2) = \delta_{\text{lat}}(\mathbf{x}) + \int_0^s dt (\nabla^2 + k^2) \tilde{\mathcal{K}}(t, \mathbf{x}; k^2). \quad (\text{D}\cdot 5)$$

This identity gives an expression for Green's function as

$$\begin{aligned} G(\mathbf{x}; k^2) &\equiv -(\nabla^2 + k^2)^{-1} \tilde{\mathcal{K}}(s, \mathbf{x}; k^2) + \int_0^s dt \tilde{\mathcal{K}}(t, \mathbf{x}; k^2) \\ &= -e^{sk^2} (\nabla^2 + k^2)^{-1} \mathcal{K}(s, \mathbf{x}) + \int_0^s dt e^{tk^2} \mathcal{K}(t, \mathbf{x}). \end{aligned} \quad (\text{D}\cdot 6)$$

By inserting Eq. (D·2), we have

$$\begin{aligned} G(\mathbf{x}; k^2) &= \frac{e^{sk^2}}{L^3} \sum_{\mathbf{n} \in \mathbf{Z}^3} \frac{\exp(-s(2\pi/L)^2 \mathbf{n}^2 + 2\pi i \mathbf{n} \cdot \mathbf{x}/L)}{(2\pi/L)^2 \mathbf{n}^2 - k^2} \\ &\quad + \int_0^s dt \frac{e^{tk^2}}{(4\pi t)^{3/2}} \sum_{\mathbf{p} \in \mathbf{Z}^3} \exp\left(-\frac{1}{4t} (\mathbf{x} - \mathbf{p}L)^2\right), \end{aligned} \quad (\text{D}\cdot 7)$$

where, in the second term, we used Poisson's summation formula

$$\sum_{\mathbf{n} \in \mathbf{Z}} \exp\left(-\frac{\mathbf{n}^2}{2\beta} + i\mathbf{n}\theta\right) = \sqrt{2\pi\beta} \sum_{\mathbf{p} \in \mathbf{Z}} \exp\left(-\frac{\beta}{2} (\theta + 2\pi\mathbf{p})^2\right). \quad (\text{D}\cdot 8)$$

The convergence of the summations and the integration in Eq. (D·7) is quite good except at $\mathbf{p} = \mathbf{0}$, where the integration in the second term has to be done analytically for $t \sim 0$. For this purpose, we use the formula

$$\frac{1}{4\pi r} = \int_0^\infty \frac{dt}{(4\pi t)^{3/2}} \exp\left(-\frac{r^2}{4t}\right), \quad (\text{D}\cdot 9)$$

and the integration can be evaluated as

$$\begin{aligned} &\int_0^s \frac{dt e^{tk^2}}{(4\pi t)^{3/2}} \exp\left(-\frac{1}{4t} \mathbf{x}^2\right) \\ &= \frac{1}{4\pi |\mathbf{x}|} - \int_0^s \frac{dt}{(4\pi t)^{3/2}} (e^{tk^2} - 1) \exp\left(-\frac{\mathbf{x}^2}{4t}\right) - \int_s^\infty \frac{dt}{(4\pi t)^{3/2}} \exp\left(-\frac{\mathbf{x}^2}{4t}\right). \end{aligned} \quad (\text{D}\cdot 10)$$

Note that s dependences in Eq. (D·6) and Eq. (D·7) cancel out on the right-hand side, and s plays a role of the cutoff λ of Eq. (D.2) in Ref. 15) as $s \sim 1/\lambda^2$. It controls the convergence of the summation in the first term in Eq. (D·7).

References

- 1) <http://nn-online.org/>
- 2) M. Taketani et al., Prog. Theor. Phys. Suppl. No. 39 (1967), 1.
N. Hoshizaki et al., Prog. Theor. Phys. Suppl. No. 42 (1968), 1.
G. E. Brown and A. D. Jackson, *Nucleon-nucleon Interaction* (North-Holland, Amsterdam, 1976).
R. Machleidt, Adv. Nucl. Phys. **19** (1989), 189.
R. Machleidt and I. Slaus, J. of Phys. G **27** (2001), R69.
- 3) R. Machleidt, Phys. Rev. C **63** (2001), 024001.
- 4) R. B. Wiringa, V. G. J. Stoks and R. Schiavilla, Phys. Rev. C **51** (1995), 38.
- 5) V. G. J. Stoks, R. A. M. Klomp, C. P. F. Terheggen and J. J. de Swart, Phys. Rev. C **49** (1994), 2950.
- 6) S. Weinberg, Phys. Lett. B **251** (1990), 288; Nucl. Phys. B **363** (1991), 3.
P. F. Bedaque and U. van Kolck, Ann. Rev. Nucl. Part. Sci. **52** (2002), 339.
- 7) Reviewed in R. Machleidt, arXiv:0704.0807.
E. Epelbaum, H. W. Hammer and U. G. Meissner, arXiv:0811.1338.
- 8) H. Yukawa, Proc. Math.-Phys. Soc. Jpn. **17** (1935), 48.
- 9) R. Jastrow, Phys. Rev. **81** (1951), 165.
- 10) R. Tamagaki et al., Prog. Theor. Phys. Suppl. No. 112 (1993), 1.
H. Heiselberg and V. Pandharipande, Annu. Rev. Nucl. Part. Sci. **50** (2000), 481.
J. M. Lattimer and M. Prakash, Phys. Rep. **333** (2000), 121.
- 11) F. Myhrer and J. Wroldsen, Rev. Mod. Phys. **60** (1988), 629.
M. Oka, K. Shimizu and K. Yazaki, Prog. Theor. Phys. Suppl. No. 137 (2000), 1.
Y. Fujiwara, Y. Suzuki and C. Nakamoto, Prog. Part. Nucl. Phys. **58** (2007), 439.
- 12) Y. Nambu, Phys. Rev. **106** (1957), 1366.
- 13) A. Jackson, A. D. Jackson and V. Pasquier, Nucl. Phys. A **432** (1985), 567.
H. Yabu and K. Ando, Prog. Theor. Phys. **74** (1985), 750.
- 14) S. Otsuki, R. Tamagaki and M. Yasuno, Prog. Theor. Phys. Suppl. Extra Number (1965), 578.
S. Machida and M. Namiki, Prog. Theor. Phys. **33** (1965), 125.
V. G. Neudachin, Yu. F. Smirnov and R. Tamagaki, Prog. Theor. Phys. **58** (1977), 1072.
D. A. Liberman, Phys. Rev. D **16** (1977), 1542.
C. DeTar, Phys. Rev. D **19** (1979), 1451.
M. Oka and K. Yazaki, Phys. Lett. B **90** (1980), 41; Prog. Theor. Phys. **66** (1981), 556;
Prog. Theor. Phys. **66** (1981), 572.
H. Toki, Z. Phys. A **294** (1980), 173.
A. Faessler, F. Fernandez, G. Lubeck and K. Shimizu, Phys. Lett. B **112** (1982), 201.
- 15) M. Lüscher, Nucl. Phys. B **354** (1991), 531.
- 16) D. Arndt, S. R. Beane and M. J. Savage, Nucl. Phys. A **726** (2003), 339.
T. T. Takahashi, T. Doi and H. Suganuma, AIP Conf. Proc. **842** (2006), 249, hep-lat/0601006.
- 17) P. de Forcrand and M. Fromm, arXiv:0907.1915.
- 18) M. Fukugita, Y. Kuramashi, M. Okawa, H. Mino and A. Ukawa, Phys. Rev. D **52** (1995), 3003, hep-lat/9501024.
- 19) S. R. Beane, P. F. Bedaque, K. Orginos and M. J. Savage, Phys. Rev. Lett. **97** (2006), 012001, hep-lat/0602010.
- 20) N. Ishii, S. Aoki and T. Hatsuda, Phys. Rev. Lett. **99** (2007), 022001, nucl-th/0611096.
- 21) S. Aoki, T. Hatsuda and N. Ishii, Comput. Sci. Disc. **1** (2008), 015009, arXiv:0805.2462.
- 22) T. Koehler, K. Goral and P. S. Julianne, Rev. Mod. Phys. **78** (2006), 1311, cond-mat/0601420.
- 23) Y. Kuramashi, Prog. Theor. Phys. Suppl. No. 122 (1996), 153, hep-lat/9510025.
- 24) H. Nemura, N. Ishii, S. Aoki and T. Hatsuda, Phys. Lett. B **673** (2009), 136, arXiv:0806.1094.
- 25) S. Okubo and R. E. Marshak, Ann. of Phys. **4** (1958), 166.
- 26) R. Tamagaki and W. Watari, Prog. Theor. Phys. Suppl. No. 39 (1967), 23.
- 27) J. Fujita and H. Miyazawa, Prog. Theor. Phys. **17** (1957), 360.
- 28) S. Weinberg, Phys. Lett. B **295** (1992), 114, hep-ph/9209257.
- 29) S. C. Pieper, V. R. Pandharipande, R. B. Wiringa and J. Carlson, Phys. Rev. C **64** (2001),

- 014001, nucl-th/0102004.
- 30) A. Akmal, V. R. Pandharipande and D. G. Ravenhall, Phys. Rev. C **58** (1998), 1804, nucl-th/9804027.
 - 31) T. Furumoto, Y. Sakuragi and Y. Yamamoto, Phys. Rev. C **79** (2009), 011601.
 - 32) M. Lüscher, Commun. Math. Phys. **105** (1986), 153.
 - 33) K. Nishijima, Phys. Rev. **111** (1958), 995.
 W. Zimmermann, Nuovo Cim. **10** (1958), 597.
 R. Haag, Phys. Rev. **112** (1958), 669.
 For a brief review, see W. Zimmermann, MPI-PAE/PTh-61/87 (1987), unpublished.
 - 34) J. N. Labrenz and S. R. Sharpe, Phys. Rev. D **54** (1996), 4595, hep-lat/9605034.
 - 35) S. R. Beane and M. J. Savage, Phys. Lett. B **535** (2002), 177.
 - 36) T. Hatsuda, Nucl. Phys. B **329** (1990), 376.
 - 37) S. Aoki et al. (CP-PACS Collaboration), Phys. Rev. D **71** (2005), 094504.
 - 38) N. Ishizuka, arXiv:0910.2772.
 - 39) N. Ishii, S. Aoki and T. Hatsuda (PACS-CS Collaboration), PoS(LATTICE 2008)155, arXiv:0903.5497.
 - 40) M. Fukugita, Y. Kuramashi, M. Okawa, H. Mino and A. Ukawa, Phys. Rev. D **52** (1995), 3003.
 - 41) E. Epelbaum, Prog. Part. Nucl. Phys. **57** (2006), 654, nucl-th/0509032.
 - 42) S. Aoki, J. Balog, T. Hatsuda, N. Ishii, K. Murano, H. Nemura and P. Weisz, PoS(LATTICE 2008)152, arXiv:0812.0673.
 - 43) S. Aoki, J. Balog and P. Weisz, Prog. Theor. Phys. **121** (2009), 1003.
 - 44) H. Nemura, N. Ishii, S. Aoki and T. Hatsuda (PACS-CS Collaboration), PoS(LATTICE 2008)156, arXiv:0902.1251.
 - 45) Y. Kuramashi, PoS(LATTICE 2008)018, arXiv:0811.2630.
 - 46) M. Jacob and G. C. Wick, Ann. of Phys. **7** (1959), 404.
 - 47) C. J. D. Lin, G. Martinelli, C. T. Sachrajda and M. Testa, Nucl. Phys. B **619** (2001), 467.
 - 48) N. Hoshizaki, Prog. Theor. Phys. Suppl. No. 42 (1968), 107.